Efficient on-the-fly ab initio semiclassical method for computing time-resolved nonadiabatic electronic spectra with surface hopping or Ehrenfest dynamics

Tomáš Zimmermann and Jií Vaníek

Citation: The Journal of Chemical Physics **141**, 134102 (2014); doi: 10.1063/1.4896735
View online: http://dx.doi.org/10.1063/1.4896735
View Table of Contents: http://scitation.aip.org/content/aip/journal/jcp/141/13?ver=pdfcov
Published by the AIP Publishing

Articles you may be interested in

On-the-fly ab initio semiclassical dynamics: Identifying degrees of freedom essential for emission spectra of oligothiophenes
J. Chem. Phys. **140**, 244114 (2014); 10.1063/1.4884718

Excited state dynamics in SO2. III. An ab initio quantum study of single- and multi-photon ionization
J. Chem. Phys. **140**, 204303 (2014); 10.1063/1.4875037

Evaluation of the importance of spin-orbit couplings in the nonadiabatic quantum dynamics with quantum fidelity and with its efficient “on-the-fly” ab initio semiclassical approximation
J. Chem. Phys. **137**, 22A516 (2012); 10.1063/1.4738878

On-the-fly ab initio molecular dynamics with multiconfigurational Ehrenfest method
J. Chem. Phys. **137**, 22A506 (2012); 10.1063/1.4734313

Photolysis of n -butyl nitrite and isoamyl nitrite at 355 nm: A time-resolved Fourier transform infrared emission spectroscopy and ab initio study
J. Chem. Phys. **130**, 174314 (2009); 10.1063/1.3129806

AIP | Chaos
CALL FOR APPLICANTS
Seeking new Editor-in-Chief

This article is copyrighted as indicated in the article. Reuse of AIP content is subject to the terms at: http://scitation.aip.org/termsconditions. Downloaded to IP: 128.178.54.130 On: Fri, 03 Oct 2014 12:49:48

Efficient on-the-fly *ab initio* semiclassical method for computing time-resolved nonadiabatic electronic spectra with surface hopping or Ehrenfest dynamics

Tomáš Zimmermann and Jiří Vaníček[a)]
Laboratory of Theoretical Physical Chemistry, Institut des Sciences et Ingénierie Chimiques, Ecole Polytechnique Fédérale de Lausanne (EPFL), CH-1015 Lausanne, Switzerland

(Received 7 January 2014; accepted 18 September 2014; published online 2 October 2014)

We derive a somewhat crude, yet very efficient semiclassical approximation for computing nonadiabatic spectra. The resulting method, which is a generalization of the multiple-surface dephasing representation, includes quantum effects through interference of mixed quantum-classical trajectories and through quantum treatment of the collective electronic degree of freedom. The method requires very little computational effort beyond the fewest-switches surface hopping or Ehrenfest locally mean-field dynamics and is very easy to implement. The proposed approximation is tested by computing the absorption and time-resolved stimulated emission spectra of pyrazine using the four-dimensional three-surface model which allows for comparison with the numerically exact quantum spectra. As expected, the multiple-surface dephasing representation is not suitable for high-resolution linear spectra, yet it seems to capture all the important features of pump-probe spectra. Finally, the method is combined with on-the-fly *ab initio* evaluation of the electronic structure (i.e., energies, forces, electric-dipole, and nonadiabatic couplings) in order to compute fully dimensional nonadiabatic spectra of pyrazine without approximations inherent to analytical, including vibronic-coupling models. The Appendix provides derivations of perturbative expressions for linear and pump-probe spectra of arbitrary mixed states and for arbitrary laser pulse shapes. © *2014 AIP Publishing LLC*. [http://dx.doi.org/10.1063/1.4896735]

I. INTRODUCTION

The vibronic spectroscopy belongs among the most important experimental tools for studying ultrafast chemical and physical processes in molecules.[1] Many different approaches ranging from simple one-photon absorption to multi-photon ultrafast time-resolved spectroscopy provide information about molecular structure, electronic states, or excited state dynamics. Analysis of such spectra requires theoretical approaches capable of attributing specific spectral features to specific dynamical processes.

The most straightforward and accurate theoretical approach is based on the direct solution of the Schrödinger equation. Unfortunately, for larger molecules this becomes quickly computationally unfeasible, and has to be replaced with some more efficient but approximate methods. In this paper, we develop such a method based on the multiple-surface dephasing representation (MSDR).[2–4] Originally used to estimate nonadiabaticity of quantum molecular dynamics, the MSDR is here generalized into a method capable of computing various linear and pump-probe electronic spectra, including those involving nonadiabatic effects. As we shall show, the proposed semiclassical method retains the efficiency and scaling properties of classical dynamics and, at the same time, captures some quantum effects on nuclear motion via the interference of (almost) classical trajectories. Because the MSDR treats the electronic degrees of freedom fully quantum-mechanically, it may also be classified as a mixed quantum-classical method.

The quantum treatment of the electronic degrees of freedom gives the MSDR the ability to describe nonadiabatic or spin-orbit couplings, which often have a strong influence on vibronic spectra.[5,6] Among the most important effects of these couplings are the line broadening due to the decay of excited state populations by internal conversion or intersystem crossing, intensity borrowing between coupled electronic states, and energy shifts of spectral peaks. However, in the presence of strong couplings in the Franck-Condon region, or in multi-photon spectroscopy, the above-mentioned effects may be difficult to separate since the couplings may change spectra completely.

The MSDR is a generalization to nonadiabatic dynamics of the dephasing representation (DR)[7–9] of quantum fidelity.[10] In the context of spectroscopy, the DR has been known as *phase-averaging*[11] and used to compute electronic spectra within the Born-Oppenheimer approximation.[11–19] The DR, which can be directly obtained by the linearization of the path integral,[20] is also closely related to the semiclassical perturbation approximation of Smith, Hubbard, and Miller[21,22] and to the linearized semiclassical initial value representation.[23] Recently, the application of the DR to Born-Oppenheimer spectra was developed further by improving the accuracy and efficiency using a semiclassical prefactor,[24,25] cellularization,[19,25] and Gaussian basis expansion.[26] Kocia and Heller have extended the method in order to compute the off-diagonal elements of the evolution operator, allowing

a)Electronic mail: jiri.vanicek@epfl.ch

 © 2014 AIP Publishing LLC

This article is copyrighted as indicated in the article. Reuse of AIP content is subject to the terms at: http://scitation.aip.org/termsconditions. Downloaded to IP: 128.178.54.130 On: Fri, 03 Oct 2014 12:49:48

its use as a general semiclassical propagator.[27] During a revision of our paper, Petit and Subotnik[28] have published a paper in which they compute linear absorption spectra of one-dimensional model potentials using a geometric average of correlation functions computed with phase averaging using trajectories propagated on either the ground or excited electronic surface, sometimes obtaining results that are even more accurate than those based on trajectories propagated on the average surface.

As will be shown later, from a pragmatic point of view probably the most appealing feature of the MSDR is the ease with which it may be incorporated into the fewest-switches surface hopping (FSSH) or Ehrenfest dynamics codes, permitting spectra calculations with very little additional programming or computational effort. Another advantage of the proposed method over wavepacket methods, typically scaling exponentially with the number of degrees of freedom, is that the number of trajectories needed for convergence is approximately independent of the number of atoms in a molecule (exactly independent in case of the DR).[29] Finally, while it does capture some quantum effects on nuclear motion, the MSDR does not require the Hessian of the potential energy, which is typically the most expensive part of semiclassical calculations.[30–36] Nevertheless, the simplicity and efficiency come at the cost of accuracy. As demonstrated in fidelity calculations, in certain cases the MSDR breaks down, even though at least the initial decay of the correlation function is usually captured correctly.[2] In the context of spectroscopy, this typically means that only the envelope of the spectrum is resolved, whereas its detailed features are missing.

To test the proposed method, absorption and time-resolved stimulated emission (TRSE) spectra of pyrazine are computed. The pyrazine molecule exhibits a conical intersection between the first (S_1) and second (S_2) bright excited states, which influences the dynamics after excitation and the resulting vibronic spectra. Because the pyrazine molecule provides an almost ideal benchmark, its vibronic spectra have been extensively studied both experimentally[37–46] and theoretically,[6,25,26,31,47–62] giving us an opportunity not only to assess the accuracy of the MSDR in relation to experiment but also to compare it with exact quantum calculations on simplified models developed by others. In addition, due to efficiency of the MSDR, we were able to go beyond simplified model systems and to compute the absorption spectrum using the *ab initio* electronic structure computed on the fly in all 24 dimensions.

The outline of the paper is as follows: in Sec. II we introduce the quantum correlation functions needed to compute the nonadiabatic linear and TRSE spectra; derivations valid for general mixed states and arbitrary laser pulse shapes are provided in the Appendix. In Sec. III, which is the core of this paper, we develop the methodology based on the MSDR to compute these correlation functions; further details on the algorithm are summarized in Sec. IV. In Sec. V, the MSDR is used to compute the absorption and TRSE spectra of pyrazine using three models: (1) a four-dimensional (4D) analytical model allowing for comparison with a numerically exact quantum mechanical result, (2) a 24-dimensional (24D) analytical model, and (3) an on-the-fly *ab initio* model based on the complete active space self-consistent field (CASSCF) method. Section VI concludes the paper.

II. NONADIABATIC SPECTRA

A. System and notation

Let us assume that the quantum dynamics of a molecule of interest depends on D nuclear degrees of freedom and is restricted to S lowest-lying electronic potential energy surfaces (PESs). As a result, the pure states of the molecule are vectors in the tensor product of electronic and nuclear Hilbert spaces, $\mathcal{H} := \mathbb{C}^S \otimes \mathcal{L}^2(\mathbb{R}^D)$, whereas mixed states as well as observables are represented by operators on the Hilbert space $\mathcal{H}$. To avoid unnecessary subscripts, we will use **bold** face for S-vectors or $S \times S$ matrices representing operators acting on the electronic Hilbert space $\mathbb{C}^S$, hat $\hat{}$ for operators acting on the nuclear Hilbert space $\mathcal{L}^2(\mathbb{R}^D)$, and arrow $\vec{}$ for vectors in the usual three-dimensional space. The scalar product is denoted simply by juxtaposition in the electronic space (as in $\mathbf{c}^\dagger\mathbf{c}$) and by a dot $\cdot$ both in the nuclear D-dimensional coordinate space and the three-dimensional space [as in $P \cdot \dot{Q}$ or $\hat{\boldsymbol{\mu}} \cdot \vec{E}(t)$].

The total Hamiltonian of the system is therefore an $S \times S$ electronic matrix of nuclear operators,

$$\hat{\mathbf{H}}_{\mathrm{tot}}(t) := \hat{\mathbf{H}} + \hat{\mathbf{V}}_{\mathrm{int}}(t), \tag{1}$$

consisting of the time-independent molecular Hamiltonian $\hat{\mathbf{H}}$ and the time-dependent potential $\hat{\mathbf{V}}_{\mathrm{int}}(t)$ describing the interaction of the molecule with a classical electromagnetic field. Within the *electric-dipole approximation*, the interaction is given by

$$\hat{\mathbf{V}}_{\mathrm{int}}(t) := -\hat{\boldsymbol{\mu}} \cdot \vec{E}(t), \tag{2}$$

where $\hat{\boldsymbol{\mu}}$ is the molecular electric dipole operator.

The exact evolution is performed with the total Hamiltonian $\hat{\mathbf{H}}_{\mathrm{tot}}(t)$. However, since we shall use extensively time-dependent perturbation theory, we will mostly need only the molecular evolution operator

$$\hat{\mathbf{U}}(t) = e^{-i\hat{\mathbf{H}}t/\hbar}. \tag{3}$$

We shall occasionally need to switch between the Schrödinger and Heisenberg pictures for the molecular evolution given by $\hat{\mathbf{U}}(t)$. To distinguish between the two pictures without introducing awkward subscripts such as S or H, in the Schrödinger picture we shall explicitly denote the time dependence of density operators (or their generalizations, always denoted by a Greek letter $\hat{\boldsymbol{\rho}}$, but possibly with a subscript, such as $\hat{\boldsymbol{\rho}}_\mu$),

$$\hat{\boldsymbol{\rho}}(t) := \hat{\mathbf{U}}(t)\hat{\boldsymbol{\rho}}\hat{\mathbf{U}}(t)^\dagger, \tag{4}$$

whereas operators corresponding to observables will have no time dependence (e.g., $\hat{\mathbf{A}}$). In the Heisenberg picture, in contrast, we shall explicitly denote the time dependence for operators representing observables, such as

$$\hat{\mathbf{A}}(t) := \hat{\mathbf{U}}(t)^\dagger\hat{\mathbf{A}}\hat{\mathbf{U}}(t), \tag{5}$$

but not for time-independent density operators or their generalizations, such as $\hat{\boldsymbol{\rho}}$ or $\hat{\boldsymbol{\rho}}_\mu$. For the total Hamiltonian (1), we

This article is copyrighted as indicated in the article. Reuse of AIP content is subject to the terms at: http://scitation.aip.org/termsconditions. Downloaded to IP: 128.178.54.130 On: Fri, 03 Oct 2014 12:49:48

shall also use the interaction picture, which will be denoted with an explicit subscript I.

Finally, we will use the following convention for the forward and inverse Fourier transforms:

$$\tilde{f}(\omega) := \frac{1}{2\pi}\int_{-\infty}^{\infty} f(t)\, e^{i\omega t} dt, \qquad f(t) = \int_{-\infty}^{\infty} \tilde{f}(\omega)\, e^{-i\omega t} d\omega. \tag{6}$$

B. Linear electric-dipole spectrum

Experimentally, the electric-dipole spectrum $\sigma(\omega)$ of a molecule can be measured from the Beer-Lambert law as the cross section $\sigma(\omega) = -\frac{1}{n_0 z}\ln[I(\omega, z)/I(\omega, 0)]$, where $I(\omega, z) := 2\pi|\vec{\tilde{E}}(\omega, z)|^2$ is the intensity (more precisely, "intensity spectral density") of the detected signal that has passed through a sample of thickness z, $I(\omega, 0)$ the intensity of the incoming radiation, and n_0 the number density of molecules in the sample. Let us assume a linearly polarized laser field $\vec{E}(t) := \vec{\epsilon}E(t)$, with amplitude $E(t)$ and unit polarization vector $\vec{\epsilon}$ ($\vec{\epsilon}\cdot\vec{\epsilon} = 1$). To avoid unnecessary arrows, let us define a projection

$$\hat{\boldsymbol{\mu}} := \hat{\vec{\boldsymbol{\mu}}}\cdot\vec{\epsilon}, \tag{7}$$

of the dipole operator onto the polarization of the laser field, keeping in mind that in an isotropic sample one has to average observable quantities over all orientations of the molecule at the end of the calculation.

As shown for general mixed states and arbitrary pulse shapes in the Appendix, within the first-order *time-dependent perturbation theory* (TDPT), the linear spectrum can be computed as[63]

$$\sigma^{(1)}(\omega) = \frac{4\pi\omega}{\hbar c}\,\mathrm{Re}\int_0^{\infty}\left[C_\mu^{(1)}(t)^* - C_\mu^{(1)}(t)\right]e^{i\omega t}dt \tag{8}$$

from the dipole time-autocorrelation function

$$C_\mu^{(1)}(t) := \mathrm{Tr}[\hat{\boldsymbol{\rho}}\,\hat{\boldsymbol{\mu}}\,\hat{\boldsymbol{\mu}}(t)], \tag{9}$$

where the initial density is assumed to be the Boltzmann equilibrium density, $\hat{\boldsymbol{\rho}} = e^{-\beta\hat{\mathbf{H}}}/\mathrm{Tr}(e^{-\beta\hat{\mathbf{H}}})$, which is stationary under evolution with $\hat{\mathbf{H}}$, i.e.,

$$\hat{\boldsymbol{\rho}}(t) = \hat{\boldsymbol{\rho}}. \tag{10}$$

The beauty of linear response theory lies in the fact that the perturbative expression (8) only depends on the dynamics of the molecule in the absence of the field. Since the dependence on the electromagnetic field cancels completely, expression (8) for the linear spectrum is valid both for continuous-wave and pulsed experiments with pulses of arbitrary length and shape.

After averaging over orientations of molecules in a given sample (see Subsection IV A), Eq. (8) describes several types of one-photon spectra: diagonal elements of $\hat{\boldsymbol{\mu}}$ give rise to rovibrational spectra, whereas the off-diagonal elements of $\hat{\boldsymbol{\mu}}$, the so-called transition dipole moments, determine vibronic spectra, the main focus of the present paper. In addition, Eq. (8) describes both absorption and emission processes, which correspond, respectively, to the first and second complex conjugate terms in Eq. (8). Note that according to Eq. (8) emission spectra have a negative sign; by convention, the sign may be changed to positive when there is no danger of confusion. One often simplifies Eq. (8) by adopting the *rotating wave approximation* (RWA) which consists in neglecting highly oscillatory terms that give negligible contribution to the spectrum. For example, to describe the vibronic absorption from the electronic ground state, the second term in Eq. (8) corresponding to emission from the ground state may be safely neglected. In contrast, to describe purely vibrational or rotational spectra of equilibrium states, the two terms may be merged, yielding an additional prefactor $1 - e^{-\beta\hbar\omega}$.

C. Pump-probe electric-dipole spectrum

Let us consider a pump-probe experiment with the heterodyne detection in the direction of the probe beam. The laser field consists of two linearly polarized pulses,

$$\vec{E}(t) := \vec{E}^{\mathrm{pu}}(t) + \vec{E}^{\mathrm{pr}}(t) := \vec{\epsilon}^{\mathrm{pu}}E^{\mathrm{pu}}(t) + \vec{\epsilon}^{\mathrm{pr}}E^{\mathrm{pr}}(t), \tag{11}$$

the pump (pu) pulse propagating in the direction $\vec{k}^{\mathrm{pu}}$ and centered at time zero, and the probe (pr) pulse propagating in the direction $\vec{k}^{\mathrm{pr}}$ and centered at a delay time τ,

$$E^{\mathrm{pu}}(t) := E_e^{\mathrm{pu}}(t)\delta_n^{\mathrm{pu}}(t), \tag{12}$$

$$E^{\mathrm{pr}}(t) := E_e^{\mathrm{pr}}(t)\delta_n^{\mathrm{pr}}(t-\tau). \tag{13}$$

Above, δ_n is an envelope of the pulse which is long on the electronic time scale, while E_e is a factor changing rapidly on the electronic time scale. Notation δ_n was used since we will later assume ultrashort pulses (of arbitrary shape), which are short on the nuclear time scale. $E_e(t)$ has usually a harmonic time dependence $\propto\cos(\omega_c t - \varphi)$, where ω_c is the carrier frequency, but let us also keep it general. In the limit of ultrashort pulses considered below, the combination of factors $E_e(t)$ and $\delta_n(t)$ in the expression for the electromagnetic pulse allows for selective excitation of specific electronic levels while preserving the delta pulse character on the nuclear time scale. To simplify notation, let us again define the projections of the electric dipole moment along the polarization of the pump and probe fields

$$\hat{\boldsymbol{\mu}}^{\mathrm{pu}} := \hat{\vec{\boldsymbol{\mu}}}\cdot\vec{\epsilon}^{\mathrm{pu}}, \tag{14}$$

$$\hat{\boldsymbol{\mu}}^{\mathrm{pr}} := \hat{\vec{\boldsymbol{\mu}}}\cdot\vec{\epsilon}^{\mathrm{pr}}. \tag{15}$$

Experimentally, the differential pump-probe spectrum is obtained as the cross section

$$\sigma(\omega, \tau) := -\frac{1}{n_0 z}\ln[I^{\mathrm{pu+pr}}(\omega, \tau, z)/I^{\mathrm{pr}}(\omega, z)], \tag{16}$$

where $I^{\mathrm{pu}+\mathrm{pr}}(\omega, \tau, z)$ is the intensity of the detected signal that has passed through a sample of thickness z in the direction of the probe when the pump pulse is present, whereas

This article is copyrighted as indicated in the article. Reuse of AIP content is subject to the terms at: http://scitation.aip.org/termsconditions. Downloaded to IP: 128.178.54.130 On: Fri, 03 Oct 2014 12:49:48

$I^{\mathrm{pr}}(\omega, z)$ is the corresponding intensity in the absence of the pump pulse. As shown for general mixed states and arbitrary pulse shapes in the Appendix, using the third-order TDPT and assuming the *nonoverlapping pulses* (NOP), *ultrashort pulse* (USP) approximation, *resonance condition* (RC), and *phase matching* (PM), the differential pump-probe spectrum can be computed as

$$\sigma^{(3)}(\omega, \tau) = \frac{4\pi\omega}{\hbar c}\mathrm{Re}\int_0^\infty \left[C^{(3)}_{\mu,\tau}(t')^* - C^{(3)}_{\mu,\tau}(t')\right]e^{i\omega t'}dt', \tag{17}$$

where $t' := t - \tau$ is the time elapsed after the probe pulse and

$$C^{(3)}_{\mu,\tau}(t') := \mathrm{Tr}[\hat{\boldsymbol{\rho}}^{\mathrm{pu}}(\tau)\hat{\boldsymbol{\mu}}^{\mathrm{pr}}\hat{\boldsymbol{\mu}}^{\mathrm{pr}}(t')] \tag{18}$$

is the third-order dipole autocorrelation function. Equation (18) has a nice interpretation as the linear autocorrelation (9) with a nonstationary initial density $\hat{\boldsymbol{\rho}}^{\mathrm{pu}}(\tau)$.[63,64] This density is obtained by a free evolution for time τ of the second-order density $\hat{\boldsymbol{\rho}}^{\mathrm{pu}}$ generated by the pump pulse, which for systems treated in this paper (which are initially in the electronic ground state, $\hat{\boldsymbol{\rho}} = \hat{\rho}_{00}|0\rangle\langle 0|$), is given by

$$\hat{\boldsymbol{\rho}}^{\mathrm{pu}} = 2\pi^2\hbar^{-2}\,\mathrm{Tr}\left[\hat{\boldsymbol{\mu}}^{\mathrm{pu}}_{\mathrm{RC}}, \left[\hat{\boldsymbol{\rho}}, \hat{\boldsymbol{\mu}}^{\mathrm{pu}}_{\mathrm{RC}}\right]\right], \tag{19}$$

where $\hat{\boldsymbol{\mu}}^{\mathrm{pu}}_{\mathrm{RC}}$ is the resonant dipole moment operator whose matrix element between electronic states k and l is scaled by the Fourier component of the pump electric field at the transition frequency ω_{kl},

$$\hat{\boldsymbol{\mu}}^{\mathrm{pu}}_{\mathrm{RC}} := \sum_{kl}\tilde{E}^{\mathrm{pu}}(\omega_{kl})\hat{\mu}^{\mathrm{pu}}_{kl}|k\rangle\langle l|. \tag{20}$$

(See the Appendix for details as well as for the treatment of more general initial states.)

By expanding the commutator in the expression (19) for the nonstationary density $\hat{\boldsymbol{\rho}}^{\mathrm{pu}}$, one finds that the third-order correlation function (18) consists of three different terms,

$$C^{(3)}_{\mu,\tau} = 2\pi^2\hbar^{-2}\left(2C^{(3)}_{\mu,\tau,\mathrm{m}} - C^{(3)}_{\mu,\tau,\mathrm{l}} - C^{(3)}_{\mu,\tau,\mathrm{r}}\right). \tag{21}$$

The three components $C^{(3)}_{\mu,\tau,y}$ (with $y = \mathrm{m}, \mathrm{l}, \mathrm{r}$) are computed in a similar fashion to Eq. (18) as

$$C^{(3)}_{\mu,\tau,y}(t') = \mathrm{Tr}[\hat{\boldsymbol{\rho}}_{\mu\mu,y}(\tau)\hat{\boldsymbol{\mu}}^{\mathrm{pr}}\hat{\boldsymbol{\mu}}^{\mathrm{pr}}(t')], \tag{22}$$

where the generalized initial "density operators" $\hat{\boldsymbol{\rho}}_{\mu\mu,y}$ are defined as

$$\hat{\boldsymbol{\rho}}_{\mu\mu,\mathrm{m}} := \hat{\boldsymbol{\mu}}^{\mathrm{pu}}_{\mathrm{RC}}\hat{\boldsymbol{\rho}}\hat{\boldsymbol{\mu}}^{\mathrm{pu}}_{\mathrm{RC}}, \tag{23}$$

$$\hat{\boldsymbol{\rho}}_{\mu\mu,\mathrm{l}} := \hat{\boldsymbol{\rho}}\hat{\boldsymbol{\mu}}^{\mathrm{pu}}_{\mathrm{RC}}\hat{\boldsymbol{\mu}}^{\mathrm{pu}}_{\mathrm{RC}}, \tag{24}$$

$$\hat{\boldsymbol{\rho}}_{\mu\mu,\mathrm{r}} := \hat{\boldsymbol{\mu}}^{\mathrm{pu}}_{\mathrm{RC}}\hat{\boldsymbol{\mu}}^{\mathrm{pu}}_{\mathrm{RC}}\hat{\boldsymbol{\rho}}. \tag{25}$$

In Eqs. (23)–(25), $y = \mathrm{m}, \mathrm{l}, \mathrm{r}$ indicates the position of $\hat{\boldsymbol{\rho}}$ with respect to the product $\hat{\boldsymbol{\mu}}^{\mathrm{pu}}_{\mathrm{RC}}\hat{\boldsymbol{\mu}}^{\mathrm{pu}}_{\mathrm{RC}}$: $\mathrm{m} = \mathrm{middle}, \mathrm{l} = \mathrm{left}, \mathrm{r} = \mathrm{right}$. In the typical setting, where $\hat{\boldsymbol{\rho}}$ is the Boltzmann density on the electronic ground state,[65] the first term of Eq. (21) generates the TRSE signal, whereas its complex conjugate in Eq. (17) corresponds to the excited-state absorption (transient absorption) signal if the electronic state excited by the pump pulse is coupled to another electronic state lying approximately $\hbar\omega_c$ higher in energy. The remaining two terms in Eq. (21) are usually negligible and vanish exactly within the rotating wave approximation since they correspond to the emission from the ground state, whereas their two complex conjugates in Eq. (17) describe the so-called "bleach" or the stimulated Raman contribution.[66] Within the Condon approximation, the bleach is nothing else than the depletion of the absorption signal due to excitation of the ground state. If the Condon approximation breaks down and the pump pulse couples to the nuclear motion directly, it is more appropriate to speak of the stimulated Raman signal. In the following, we will concentrate only on the TRSE term; the transient absorption and stimulated Raman contributions, which are important experimentally, can be computed in a like manner.

III. MSDR FOR NONADIABATIC SPECTRA

The MSDR (Ref. 2) was originally developed as a semiclassical approximation to estimate the nonadiabaticity of quantum molecular dynamics, measured by the overlap $\langle\Psi_{\mathrm{BO}}(t)|\Psi_{\mathrm{full}}(t)\rangle$ of the Born-Oppenheimer and full nonadiabatic molecular wavefunctions. This overlap is a special case of quantum fidelity amplitude[9,10] $f_{\mathrm{QM}}(t) = \mathrm{Tr}(\hat{\boldsymbol{\rho}}e^{+i\hat{\mathbf{H}}_0 t/\hbar}e^{-i\hat{\mathbf{H}}_\epsilon t/\hbar})$ which is a measure of stability of quantum dynamics under a perturbation present in $\hat{\mathbf{H}}_\epsilon$ but absent in $\hat{\mathbf{H}}_0$. In the case of nonadiabaticity, e.g., $\hat{\mathbf{H}}_0$ is the Born-Oppenheimer Hamiltonian and $\hat{\mathbf{H}}_\epsilon$ the full nonadiabatic Hamiltonian. Since the quantum fidelity amplitude $f_{\mathrm{QM}}(t)$ can be thought of as a specific correlation function, here we generalize the MSDR to describe dipole time-autocorrelation functions needed in calculations of the nonadiabatic linear and pump-probe spectra. Instead of $f_{\mathrm{QM}}(t)$, we want to evaluate Eq. (9) for the linear spectra or Eq. (22) for the pump-probe spectra. First, let us consider the linear spectrum and transform Eq. (9) from the Heisenberg to Schrödinger picture

$$C^{(1)}_{\mu}(t) = \mathrm{Tr}[\hat{\boldsymbol{\rho}}_{\mu}(t)\hat{\boldsymbol{\mu}}], \tag{26}$$

where we introduced new operator

$$\hat{\boldsymbol{\rho}}_{\mu} := \hat{\boldsymbol{\rho}}\hat{\boldsymbol{\mu}}. \tag{27}$$

As in the derivation of the original MSDR method, $C^{(1)}_{\mu}(t)$ is partially Wigner transformed[67] over nuclear degrees of freedom, yielding the exact expression

$$C^{(1)}_{\mu}(t) = h^{-D}\int d^{2D}X\,\mathrm{Tr}_e[\boldsymbol{\rho}_{\mu,\mathrm{W}}(X,t)\boldsymbol{\mu}_{\mathrm{W}}(X)], \tag{28}$$

where X denotes the point (Q, P) in the $2D$-dimensional nuclear phase space, Tr_e is the trace over electronic degrees of freedom, and a partial Wigner transform of an operator $\hat{\mathbf{A}}$ is given by

$$\mathbf{A}_{\mathrm{W}}(X) := \int d^D\xi\,\langle Q - \xi/2|\hat{\mathbf{A}}|Q + \xi/2\rangle\, e^{i\xi\cdot P/\hbar}. \tag{29}$$

To obtain the MSDR, the exact evolution of $\boldsymbol{\rho}_{\mu,\mathrm{W}}(X,t)$ is replaced with an approximate propagation scheme Z using either the locally mean-field dynamics ($Z = \mathrm{LMFD}$),[2] or the

This article is copyrighted as indicated in the article. Reuse of AIP content is subject to the terms at: http://scitation.aip.org/termsconditions. Downloaded to IP: 128.178.54.130 On: Fri, 03 Oct 2014 12:49:48

fewest-switches surface hopping ($Z = \text{FSSH}$)[68]

$$C^{(1)}_{\mu,\text{MSDR},Z}(t) = h^{-D}\int d^{2D}X\,\text{Tr}_e[\boldsymbol{\rho}_{\mu,\text{W},Z}(X,t)\boldsymbol{\mu}_\text{W}(X)] = h^{-D}\int d^{2D}X\,\text{Tr}_e\{\boldsymbol{\rho}_{\mu,\text{W},Z}[X_Z(t),t]\boldsymbol{\mu}_\text{W}[X_Z(t)]\}. \quad (30)$$

Equation (30) is evaluated by using the propagation scheme Z to evolve $\boldsymbol{\rho}_{\mu,\text{W},Z}$ together with phase-space trajectories $X_Z(t)$ with initial conditions $X_Z(0) := X$; note that in the second line of Eq. (30), we used that the Jacobian $\det[\partial X_Z(t)/\partial X] = 1$. (The propagation methods are described in detail in Subsections III A–III F, while their numerical implementation is presented in Subsection IV C.) To evaluate the integral (30), the trace of products of complex matrices is taken for each trajectory and the resulting complex numbers are summed over trajectories. This sum is responsible for the interference effects which allow recovering some of the quantum effects on the nuclear dynamics.

The ability to use two complementary propagation methods (LMFD and FSSH) in the same framework is advantageous; indeed, the two methods are best suited for two very different limiting situations:[69] the LMFD performs the best for the dynamics occurring within a region of extended coupling and may fail after a single passage of a localized coupling region—situation where the FSSH works well. Vice versa, the FSSH may fail in the regions of extended coupling or when the coupling region is visited repeatedly during the dynamics.

The main difference from standard use of the LMFD or FSSH is that Eq. (30) requires propagating the partial Wigner transform of $\hat{\boldsymbol{\rho}}_\mu = \hat{\boldsymbol{\rho}}\hat{\boldsymbol{\mu}}$, and not the usual density operator $\hat{\boldsymbol{\rho}}$. Still, it will be easier to present the algorithm after first reviewing the standard propagation of $\boldsymbol{\rho}_\text{W}$; in fact, as will be shown later, a simultaneous propagation of $\boldsymbol{\rho}_\text{W}$ is required in the MSDR_0 variant of our method to obtain the force with which to propagate $\boldsymbol{\rho}_{\mu,\text{W}}$.

A. Propagation of density matrix $\boldsymbol{\rho}_\text{W}$ with LMFD or FSSH

A rather accurate approximation for propagating $\boldsymbol{\rho}_\text{W}$ uses the mixed quantum-classical Liouville (MQCL) equation[70–76]

$$\frac{\partial\boldsymbol{\rho}_{\text{W,MQCL}}(X,t)}{\partial t} = -\frac{i}{\hbar}[\mathbf{H}_\text{W},\boldsymbol{\rho}_{\text{W,MQCL}}] + \frac{1}{2}\{\mathbf{H}_\text{W},\boldsymbol{\rho}_{\text{W,MQCL}}\} - \frac{1}{2}\{\boldsymbol{\rho}_{\text{W,MQCL}},\mathbf{H}_\text{W}\}, \quad (31)$$

where $\{\mathbf{A},\mathbf{B}\} = \frac{\partial\mathbf{A}}{\partial Q}\frac{\partial\mathbf{B}}{\partial P} - \frac{\partial\mathbf{A}}{\partial P}\frac{\partial\mathbf{B}}{\partial Q}$ is the Poisson bracket over the nuclear degrees of freedom. The LMFD and FSSH propagation schemes can be both thought of as approximate solutions of Eq. (31); in addition, both share a common feature that all elements of $\boldsymbol{\rho}_{\text{W},Z}(X,t)$ are propagated using the same PES, which may, nevertheless, differ for different trajectories.

In the diabatic basis, the LMFD is expressed as

$$\frac{\partial\boldsymbol{\rho}_{\text{W,LMFD}}(X,t)}{\partial t} = -\frac{i}{\hbar}[\mathbf{H}_\text{W},\boldsymbol{\rho}_{\text{W,LMFD}}] - F_\text{LMFD}\frac{\partial\boldsymbol{\rho}_{\text{W,LMFD}}}{\partial P} - \frac{P}{M}\frac{\partial\boldsymbol{\rho}_{\text{W,LMFD}}}{\partial Q}, \quad (32)$$

where F_LMFD is a locally mean-field force, the precise form of which will be specified below [Eq. (36)]. Equation (32) is derived from the MQCL equation (31) by invoking the mean-field approximation separately for each X; for a detailed derivation and for an analogous equation in the adiabatic basis see Ref. 2. An alternative interpretation of the LMFD (32) of $\boldsymbol{\rho}_\text{W}(X,t)$ as a dynamics of a swarm of trajectories, each propagated separately with its own Ehrenfest dynamics,[2] is obtained by combining the partial phase-space and time derivatives in Eq. (32) to form the convective (or total) derivative

$$\frac{Df}{Dt} = \frac{\partial f}{\partial t} + \dot{Q}\frac{\partial f}{\partial Q} + \dot{P}\frac{\partial f}{\partial P}. \quad (33)$$

This permits transforming Eq. (32) from the Eulerian reference frame at rest to the Lagrangian frame moving with the phase-space flow of the Hamiltonian vector field

$$(\dot{Q},\dot{P}) = (P/M, F_Z). \quad (34)$$

In the Lagrangian frame (denoted by subscript L), Eq. (32) becomes for each trajectory (whose initial condition X is suppressed below) identical to the von Neumann-Liouville equation for the single discrete electronic degree of freedom with a *time-dependent* Hamiltonian $\mathbf{H}_{\text{W,Z,L}}(t) := \mathbf{H}_\text{W}[X_Z(t)]$

$$\frac{D\boldsymbol{\rho}_{\text{W,Z,L}}(t)}{Dt} = -\frac{i}{\hbar}[\mathbf{H}_{\text{W,Z,L}}(t),\boldsymbol{\rho}_{\text{W,Z,L}}(t)]. \quad (35)$$

For each trajectory, one can easily transform back to the Eulerian frame via $\boldsymbol{\rho}_{\text{W},Z}[X_Z(t),t] = \boldsymbol{\rho}_{\text{W,Z,L}}(t)$.

Note that "LMFD" was replaced with Z in the propagation Eqs. (34) and (35) since they are valid for both LMFD and FSSH; the difference between the two schemes is mainly due to the force F_Z used:

The LMFD uses the locally mean-field force

$$F_\text{LMFD} := -\langle\partial\mathbf{H}_\text{W}/\partial Q\rangle_{e,\boldsymbol{\rho}_{\text{W,LMFD}}}, \quad (36)$$

where

$$\langle\mathbf{A}\rangle_{e,\boldsymbol{\rho}}(X,t) := \text{Tr}_e[\boldsymbol{\rho}(X,t)\mathbf{A}(X)]$$

denotes a partial average of $\mathbf{A}$ over the electronic degrees of freedom.

In the physically motivated FSSH scheme,[68] each trajectory follows the Born-Oppenheimer dynamics on one of the occupied PESs; the trajectory moving on the jth PES feels the force

$$F_\text{FSSH}(X) := -\partial H_{\text{W},jj}(X)/\partial Q. \quad (37)$$

In addition, after each time step Δt, trajectories are allowed to jump between PESs according to a stochastic hopping algorithm, where the probability of a hop from the current electronic state j to state k is given by

$$P_{jk} = \Delta t\, b_{kj}/\rho_{jj}, \quad (38)$$

This article is copyrighted as indicated in the article. Reuse of AIP content is subject to the terms at: http://scitation.aip.org/termsconditions. Downloaded to IP: 128.178.54.130 On: Fri, 03 Oct 2014 12:49:48

and $b_{kj} = -(i/\hbar)(H_{kj}\rho_{jk} - \rho_{kj}H_{jk})$.[68] (For simplicity, subscripts W and FSSH were omitted.)

B. Propagation of $\rho_{\mu,\mathrm{W}}$: MSDR$_0$ and MSDR$_\mu$

To compute dipole correlation functions with the MSDR Eq. (30), one needs to propagate $\rho_{\mu,\mathrm{W}}(X,t)$ instead of $\rho_{\mathrm{W}}(X,t)$. Whereas the propagation Eq. (35) for $\rho_{\mathrm{W}}(X,t)$ is easily generalized for $\rho_{\mu,\mathrm{W}}(X,t)$ as

$$\frac{D\rho_{\mu,\mathrm{W,Z,L}}(t)}{Dt} = -\frac{i}{\hbar}[\mathbf{H}_{\mathrm{W,Z,L}}(t), \rho_{\mu,\mathrm{W,Z,L}}(t)], \tag{39}$$

it is not immediately obvious how to compute the force F_Z determining the phase-space flow (34). In the case of LMFD, e.g., replacement of $\rho_{\mathrm{W}}(X,t)$ with $\rho_{\mu,\mathrm{W}}(X,t)$ in Eq. (36) would result in the force $F_{\mathrm{LMFD}} = -\langle\partial\mathbf{H}_{\mathrm{W}}/\partial Q\rangle_{e,\rho_{\mu,\mathrm{W,LMFD}}}$ averaged over $\rho_{\mu,\mathrm{W,\,LMFD}}(X,t)$ which would often be unphysical as the matrix $\rho_{\mu,\mathrm{W,\,LMFD}}(X,t)$ is not guaranteed to be Hermitian and positive semidefinite. This difficulty is overcome by generalizing the strategy used in the original phase-averaging method within the Born-Oppenheimer approximation[11] and in the DR: the force F_Z acting on $\rho_{\mu,\mathrm{W},Z}(X,t)$ is set to be equal either to the force acting on $\rho_{\mathrm{W},Z}(X,t)$, propagated with Eq. (35), resulting in a method that we designate MSDR$_0$, or to the force acting on $\rho_{\mu\mu,\mathrm{W,LMFD}}(X,t)$, where

$$\hat{\boldsymbol{\rho}}_{\mu\mu} := T^{-1}\hat{\boldsymbol{\mu}}\hat{\boldsymbol{\rho}}\hat{\boldsymbol{\mu}}, \tag{40}$$

$$T := \mathrm{Tr}(\hat{\boldsymbol{\mu}}\hat{\boldsymbol{\rho}}\hat{\boldsymbol{\mu}}), \tag{41}$$

resulting in a method that we designate MSDR$_\mu$. Due to the normalization constant T, the Wigner-transformed matrix $\rho_{\mu\mu,\mathrm{W}}(X)$ has unit trace, and since it is also Hermitian and positive semidefinite, it can be propagated in an analogous way to $\rho_{\mathrm{W},Z}(X,t)$ as

$$\frac{D\rho_{\mu\mu,\mathrm{W,Z,L}}(t)}{Dt} = -\frac{i}{\hbar}[\mathbf{H}_{\mathrm{W,Z,L}}(t), \rho_{\mu\mu,\mathrm{W,Z,L}}(t)], \tag{42}$$

with either the LMFD or FSSH force associated to $\rho_{\mu\mu,\mathrm{W}}(X,t)$ instead of $\rho_{\mathrm{W}}(X,t)$.

In the two-surface Born-Oppenheimer absorption spectroscopy with diagonal elements of $\boldsymbol{\mu}$ set to zero, MSDR$_0$ corresponds to the propagation on the ground PES whereas MSDR$_\mu$ employs propagation on the excited PES. [Incidentally, in this important special case, naïve averaging of the force over $\rho_{\mu,\mathrm{W,\,LMFD}}(X,t)$ would yield $F_{\mathrm{LMFD}} = 0$.]

Finally, a third type of dynamics—MSDR$_{\mathrm{av}}$—with F_Z associated to the time-evolved density $\rho_{\mathrm{av,W}}(X,t)$ with initial value $\rho_{\mathrm{av,W}}(X,0) = [\rho_{\mathrm{W}}(X) + \rho_{\mu\mu,\mathrm{W}}(X)]/2$ could be envisaged, which would correspond to the propagation on the average PES in the two-surface Born-Oppenheimer model. The possibility of using the average Hamiltonian was—for the uncoupled two-PES system—considered already in the phase-averaging method[11] and several researchers found—in the similar context—the propagation of $\rho_{\mu,\mathrm{W}}(t)$ on the average PES to be the most natural and accurate choice.[12,15–17,20,77–79] In our setting, MSDR$_{\mathrm{av}}$ is also expected to work as well as or better than the MSDR$_0$ or MSDR$_\mu$, but—in contrast to MSDR$_0$ and MSDR$_\mu$—the dynamics underlying a MSDR$_{\mathrm{av}}$ cannot be used to analyze the dynamics of the ground or excited states. The MSDR$_{\mathrm{av}}$ approach is thus not explored in detail here.

C. MSDR based on the locally mean-field dynamics

To summarize, MSDR based on the LMFD is the evaluation of Eq. (30) using $\rho_{\mu,\mathrm{W,\,LMFD}}(X,t)$ propagated with Eq. (39) in the Lagrangian frame given by the phase-space flow (34) with the locally mean-field force

$$F_{\mathrm{MSDR}_0/\mathrm{LMFD}} = -\left\langle\partial\mathbf{H}_{\mathrm{W}}/\partial Q\right\rangle_{e,\rho_{\mathrm{W,LMFD}}},$$

or

$$F_{\mathrm{MSDR}_\mu/\mathrm{LMFD}} = -\left\langle\partial\mathbf{H}_{\mathrm{W}}/\partial Q\right\rangle_{e,\rho_{\mu\mu,\mathrm{W,LMFD}}},$$

where the densities $\rho_{\mathrm{W,LMFD}}(X,t)$ and $\rho_{\mu\mu,\mathrm{W,LMFD}}(X,t)$ have initial conditions $\rho_{\mathrm{W}}(X)$ and $\rho_{\mu\mu,\mathrm{W}}(X)$, and are propagated with Eqs. (35) and (42), respectively.

D. MSDR based on the fewest-switches surface hopping

In the framework developed in Subsections III A–III C, MSDR based on the FSSH resembles closely MSDR/LMFD–the only differences are in the force and permission of hops between PESs. To summarize, MSDR based on the FSSH again consists in the evaluation of Eq. (30) using $\rho_{\mu,\mathrm{W,\,FSSH}}(X,t)$ propagated with Eq. (39) in the Lagrangian frame given by the phase-space flow (34), however, with the force

$$F_{\mathrm{MSDR}_0/\mathrm{FSSH}} = -\partial H_{\mathrm{W},jj}(X)/\partial Q,$$

or

$$F_{\mathrm{MSDR}_\mu/\mathrm{FSSH}} = -\partial H_{\mathrm{W},jj}(X)/\partial Q,$$

associated, respectively, with density $\rho_{\mathrm{W,FSSH}}(X,t)$ given initially by $\rho_{\mathrm{W}}(X)$ and propagated with Eq. (35), or with density $\rho_{\mu\mu,\mathrm{W,FSSH}}(X,t)$ given initially by $\rho_{\mu\mu,\mathrm{W}}(X)$ and propagated with Eq. (42). In addition, as mentioned in Subsection III A, hops between PESs are allowed after each time step according to Eq. (38) for $\rho_{\mathrm{W,FSSH}}$ or analogous equation for $\rho_{\mu\mu,\mathrm{W,FSSH}}$.

E. MSDR for electronically pure states

A simplified MSDR expression may be derived for electronically pure initial density $\rho_{\mathrm{W}}(X,0)$ assuming the Condon approximation $\boldsymbol{\mu}_{\mathrm{W}}(X) \approx \boldsymbol{\mu}$. To define what "electronically pure" means, $\rho_{\mathrm{W}}(X)$ is first rewritten as

$$\rho_{\mathrm{W}}(X,t) = \rho(X,t)\rho_e(X,t), \tag{43}$$

where $\rho(X,t) := \mathrm{Tr}_e\rho_{\mathrm{W}}(X,t)$ is a scalar function of X and t, and $\rho_e(X,t)$ is the conditional density matrix with the property $\mathrm{Tr}_e\rho_e(X,t) = 1$ for all X and t. The electronically pure $\rho_{\mathrm{W}}(X,t)$ is then defined by requiring the conditional electronic density matrix $\rho_e(X,t)$ to be pure for all X. An electronically pure initial density matrix can hence be written as the tensor product

$$\rho_{\mathrm{W}}(X) = \rho(X)\,\mathbf{c}(X)\otimes\mathbf{c}(X)^\dagger, \tag{44}$$

This article is copyrighted as indicated in the article. Reuse of AIP content is subject to the terms at: http://scitation.aip.org/termsconditions. Downloaded to IP: 128.178.54.130 On: Fri, 03 Oct 2014 12:49:48

where $\mathbf{c}(X)$ is an S-component column vector containing the initial electronic wave function for nuclei located at X. This is usually a good approximation at ambient temperatures due to large energy gaps between electronic states. For example, in a typical absorption experiment at room temperature, only the ground PES is occupied initially and even though the vibrational density matrix $\rho(X)$ is usually a mixed state, $\boldsymbol{\rho}_e(X)$ is well described by a pure state with only one nonzero element. Substituting Eq. (44) into Eq. (30) we arrive at

$$\begin{aligned} C^{(1)}_{\mu,\mathrm{MSDR},Z}(t) &= h^{-D}\int d^{2D}X \rho(X)\, \mathbf{c}_Z(X,t)^\dagger\, \boldsymbol{\mu}\mathbf{c}_{\mu,Z}(X,t) \\ &= h^{-D}\int d^{2D}X \rho(X)\, \mathbf{c}_Z[X_Z(t),t]^\dagger \boldsymbol{\mu}\mathbf{c}_{\mu,Z}[X_Z(t),t], \end{aligned} \quad (45)$$

where $\mathbf{c}_Z(X,0) := \mathbf{c}(X)$ and $\mathbf{c}_{\mu,Z}(X,0) := \boldsymbol{\mu}\mathbf{c}(X)$ are propagated in the Lagrangian reference frame according to the Schrödinger equations

$$\begin{aligned} D\mathbf{c}_{Z,\mathrm{L}}(t)/Dt &= -(i/\hbar)\mathbf{H}_{\mathrm{W},Z,\mathrm{L}}(t)\mathbf{c}_{Z,\mathrm{L}}(t), \\ D\mathbf{c}_{\mu,Z,\mathrm{L}}(t)/Dt &= -(i/\hbar)\mathbf{H}_{\mathrm{W},Z,\mathrm{L}}(t)\mathbf{c}_{\mu,Z,\mathrm{L}}(t). \end{aligned} \quad (46)$$

The reason why the Condon approximation permits deriving Eq. (46) is that when $\boldsymbol{\mu}$ is a constant matrix, then $\boldsymbol{\rho}_{\mu,\mathrm{W}}(X) = \boldsymbol{\rho}_{\mathrm{W}}(X)\,\boldsymbol{\mu}$. In the general case, $\hat{\boldsymbol{\rho}}$ and $\hat{\boldsymbol{\mu}}$ cannot be treated separately and the Wigner transform $(\hat{\boldsymbol{\rho}}\hat{\boldsymbol{\mu}})_{\mathrm{W}}$ must be computed explicitly. Even in the general case one may introduce an additional, possibly rather crude approximation $(\hat{\boldsymbol{\rho}}\hat{\boldsymbol{\mu}})_{\mathrm{W}}(X) \approx \boldsymbol{\rho}_{\mathrm{W}}(X)\,\boldsymbol{\mu}_{\mathrm{W}}(X)$, and thus simplify Eq. (28) by generalizing Eqs. (45) and (46) beyond the Condon approximation. Note that $\boldsymbol{\mu}_{\mathrm{W}}(X) = \boldsymbol{\mu}(Q)$ since $\hat{\boldsymbol{\mu}}$ is independent of nuclear momentum.

F. MSDR for TRSE spectra

The generalization of the MSDR to compute TRSE spectra is done along the same lines as for the linear spectra with the only exception that the initial density $\hat{\boldsymbol{\rho}}$ is replaced with $\hat{\boldsymbol{\rho}}_{\mu\mu,\mathrm{m}}(\tau)$. The remaining issue—how to compute $\boldsymbol{\rho}_{\mu\mu,\mathrm{m,W}}(X,\tau)$ with the LMFD or FSSH dynamics—is solved by realizing that $\boldsymbol{\rho}_{\mu\mu,\mathrm{m,W}}(X,0) = T\,\boldsymbol{\rho}_{\mu\mu,\mathrm{W}}(X,0)$, where the norm T is conserved during the propagation, and hence $\boldsymbol{\rho}_{\mu\mu,\mathrm{m,W}}(X,\tau)$ is obtained with Eq. (42) for propagating $\boldsymbol{\rho}_{\mu\mu,\mathrm{W}}(X,t)$. Note that also in the second step of the calculation [i.e., the actual calculation of the correlation function using a nonstationary initial state $\boldsymbol{\rho}_{\mu\mu,\mathrm{m,W}}(X,\tau)$], the norm of $\boldsymbol{\rho}_{\mu\mu,\mathrm{m,W}}(X,\tau)$ must be factored out in order to compute the average forces or hopping probabilities correctly.

Further details of the algorithm and sampling strategies are described in Subsection IV C.

IV. COMPUTATIONAL DETAILS

A. Averaging over orientations of a molecule

The expression (7) for $\hat{\boldsymbol{\mu}}$ contains the dot product $\hat{\vec{\boldsymbol{\mu}}}\cdot\vec{\epsilon}$ which depends on the orientation of the molecule and polarization of the pulse. To describe isotropic samples it is thus necessary to average over all possible relative orientations of the molecule and light polarization. When all nonzero elements of $\hat{\vec{\boldsymbol{\mu}}}$ are parallel, the averaging affects only the overall intensity of the absorption spectrum by a prefactor given by[80]

$$\frac{\int_0^{2\pi} d\varphi \int_0^{\pi} d\theta \cos^2\theta \sin\theta}{\int_0^{2\pi} d\varphi \int_0^{\pi} d\theta \sin\theta} = \frac{1}{3}, \quad (47)$$

where θ denotes the angle between $\hat{\vec{\boldsymbol{\mu}}}$ and $\vec{\epsilon}$. When all nonzero elements of $\hat{\vec{\boldsymbol{\mu}}}$ lie in the same plane (as in the case of pyrazine models studied here), the averaging over θ may still be performed analytically, and yields again the prefactor 1/3, whereas the averaging over φ must be performed numerically. In other cases, even the average over θ has to be computed numerically. As for pump-probe spectra, a similar approach can be used under the additional assumptions that both pulses have the same polarization and that the molecule does not rotate between the pulses. The latter assumption is usually justified since the rotational frequency of even the fastest-rotating molecules at room temperature lies in the terahertz range. As a result, for pump-probe spectra the analytical factor 1/3 is replaced with a factor 1/5 since

$$\frac{\int_0^{2\pi} d\varphi \int_0^{\pi} d\theta \cos^4\theta \sin\theta}{\int_0^{2\pi} d\varphi \int_0^{\pi} d\theta \sin\theta} = \frac{1}{5}. \quad (48)$$

B. Damping of the autocorrelation function

The effects of environment or neglected degrees of freedom are often accounted for by multiplying autocorrelation functions $C^{(1)}_{\mu}(t)$ and $C^{(3)}_{\mu,\tau}(t')$ by a phenomenological damping function $f_{\mathrm{damp}}(t)$. Here, we used an exponential damping function of the form

$$f_{\mathrm{damp}}(t) = \exp(-t/\tau_{\mathrm{damp}}), \quad (49)$$

which generates Lorentzian broadening of spectral peaks. We employed, respectively, $\tau_{\mathrm{damp}} = 20$, 150, and 150 fs in the 4D, 24D, and 30-dimensional (30D) pyrazine models. In the calculations of TRSE spectra, the environmental effects were entirely neglected during the typically short propagation between pump and probe pulses.

C. Algorithm

To find the nuclear trajectories determining the Lagrangian reference frame in which $\boldsymbol{\rho}_{\mu,\mathrm{W}}$ is propagated, we first rewrite the initial density matrix $\boldsymbol{\rho}^{\mathrm{init}}_{\mathrm{W}}(X)$ [given by $\boldsymbol{\rho}_{\mathrm{W}}(X)$ in MSDR_0 or by $\boldsymbol{\rho}_{\mu\mu,\mathrm{W}}(X)$ in MSDR_μ] as

$$\boldsymbol{\rho}^{\mathrm{init}}_{\mathrm{W}}(X) = \rho^{\mathrm{init}}(X)\,\boldsymbol{\rho}^{\mathrm{init}}_{e}(X), \quad (50)$$

where $\rho^{\mathrm{init}}(X) := \mathrm{Tr}_e\boldsymbol{\rho}^{\mathrm{init}}_{\mathrm{W}}(X)$. Scalar nuclear density $\rho^{\mathrm{init}}(X)$ is used as a weight for sampling the phase-space initial conditions X for N trajectories $X_Z(t)$, which are propagated either with the LMFD or FSSH dynamics (denoted again by Z). For each initial phase-space point X generated, the electronic part $\boldsymbol{\rho}^{\mathrm{init}}_{e}(X)$ satisfies $\mathrm{Tr}_e\boldsymbol{\rho}^{\mathrm{init}}_{e}(X) = 1$. Whereas X determines the initial condition of a LMFD trajectory completely, for FSSH one also needs to randomly select the initial surface for each

This article is copyrighted as indicated in the article. Reuse of AIP content is subject to the terms at: http://scitation.aip.org/termsconditions. Downloaded to IP: 128.178.54.130 On: Fri, 03 Oct 2014 12:49:48

trajectory; the probability for the initial surface of a trajectory starting at X to be surface j is given by the diagonal element $\rho^{\text{init}}_{e,jj}(X)$.

Assuming for simplicity that $(\hat{\boldsymbol{\rho}}\hat{\boldsymbol{\mu}})_{\text{W}}(X) \approx \boldsymbol{\rho}_{\text{W}}(X)\,\boldsymbol{\mu}_{\text{W}}(X)$, which follows, e.g., from the Condon approximation, von Neumann equation (39) implies that the matrix $\boldsymbol{\rho}_{e,\mu}(X,t)$ [with an initial condition $\boldsymbol{\rho}_{e,\mu}(X,0) = \boldsymbol{\rho}^{\text{init}}_{e}(X)\boldsymbol{\mu}_{\text{W}}(X)$] is propagated along each trajectory $X_Z(t)$ by successive multiplication by short-time propagators

$$\begin{aligned}&\boldsymbol{\rho}_{e,\mu,Z}[X_Z(t+\Delta t), t+\Delta t]\\ &\quad\approx \mathbf{U}_{\mathbf{H}_{\text{W}}[X_Z(t)]}(\Delta t)^{\dagger}\,\boldsymbol{\rho}_{e,\mu,Z}[X_Z(t),t]\mathbf{U}_{\mathbf{H}_{\text{W}}[X_Z(t)]}(\Delta t),\end{aligned}$$

or—in practice—in the Lagrangian frame,

$$\begin{aligned}\boldsymbol{\rho}_{e,\mu,Z,\text{L}}(t+\Delta t) \approx{}& \mathbf{U}_{\mathbf{H}_{\text{W,Z,L}}(t)}(\Delta t)^{\dagger}\,\boldsymbol{\rho}_{e,\mu,Z,\text{L}}(t)\\ &\times \mathbf{U}_{\mathbf{H}_{\text{W,Z,L}}(t)}(\Delta t),\end{aligned} \tag{51}$$

where Δt is the time step and

$$\mathbf{U}_{\mathbf{A}}(t) := e^{-i\mathbf{A}t/\hbar} \tag{52}$$

denotes a unitary evolution operator induced by a *time-independent* Hermitian operator $\mathbf{A}$. Trajectory $X_Z(t)$ starts at $X_Z(0) = X$ and is propagated with the LMFD or FSSH force associated in both MSDR_0 and MSDR_μ with the density $\boldsymbol{\rho}_{e,Z}(X,t)$, which is according to Eqs. (35) and (42) evolved with an equation analogous to Eq. (51),

$$\boldsymbol{\rho}_{e,Z,\text{L}}(t+\Delta t) \approx \mathbf{U}_{\mathbf{H}_{\text{W,Z,L}}(t)}(\Delta t)^{\dagger}\,\boldsymbol{\rho}_{e,Z,\text{L}}(t)\mathbf{U}_{\mathbf{H}_{\text{W,Z,L}}(t)}(\Delta t).$$

The MSDR approximation (30) to the correlation function $C^{(1)}_{\mu,\text{MSDR},Z}(t)$ is then computed as the arithmetic average over all N trajectories,

$$\begin{aligned}C^{(1)}_{\mu,\text{MSDR},Z}(t) &\approx \frac{1}{N}\sum_{k=1}^{N}\text{Tr}_e\{\boldsymbol{\rho}_{e,\mu,Z}[X_{k,Z}(t),t]\boldsymbol{\mu}_{\text{W}}[X_{k,Z}(t)]\}\\ &= \frac{1}{N}\sum_{k=1}^{N}\text{Tr}_e\big[\boldsymbol{\rho}_{e,\mu,Z,\text{L}_k}(t)\boldsymbol{\mu}_{\text{W,Z,L}_k}(t)\big],\end{aligned} \tag{53}$$

where L_k denotes the Lagrangian frame of kth trajectory.

For electronically pure states, i.e., states of the form $\boldsymbol{\rho}^{\text{init}}_{e}(X) \equiv \mathbf{c}^{\text{init}}(X)\otimes\mathbf{c}^{\text{init}}(X)^{\dagger}$, the propagation scheme simplifies. Instead of propagating the density matrix $\boldsymbol{\rho}_{e,\mu,Z}(X,t)$ using Eq. (51) that solves the von Neumann equation (39), two wave functions represented by vectors $\mathbf{c}_Z(X,t)$ and $\mathbf{c}_{\mu,Z}(X,t)$ with initial conditions $\mathbf{c}_Z(X,0) := \mathbf{c}^{\text{init}}(X)$ and $\mathbf{c}_{\mu,Z}(X,0) := \boldsymbol{\mu}_{\text{W}}(X)\,\mathbf{c}^{\text{init}}(X)$ are propagated by solving the Schrödinger equations (46):

$$\begin{aligned}\mathbf{c}_Z[X_Z(t+\Delta t), t+\Delta t] &\approx \mathbf{U}_{\mathbf{H}_{\text{W}}[X_Z(t)]}(\Delta t)\,\mathbf{c}_Z[X_Z(t),t],\\ \mathbf{c}_{\mu,Z}[X_Z(t+\Delta t), t+\Delta t] &\approx \mathbf{U}_{\mathbf{H}_{\text{W}}[X_Z(t)]}(\Delta t)\,\mathbf{c}_{\mu,Z}[X_Z(t),t].\end{aligned}$$

As above, the LMFD or FSSH force is associated in both MSDR_0 and MSDR_μ with the wavefunction $\mathbf{c}_Z(X,t)$, so in contrast to the situation for electronically impure states, no additional quantum propagation is required to find the force. Finally, the MSDR correlation function (30) is evaluated as

$$\begin{aligned}&C^{(1)}_{\mu,\text{MSDR},Z}(t)\\ &\quad\approx \frac{1}{N}\sum_{k=1}^{N}\mathbf{c}_Z[X_{k,Z}(t),t]^{\dagger}\boldsymbol{\mu}_{\text{W}}[X_{k,Z}(t)]\mathbf{c}_{\mu,Z}[X_{k,Z}(t),t].\end{aligned} \tag{54}$$

D. Discretization

Numerical averaging over the angle φ determining the orientation of the molecule was performed using a spacing of 30°. In the calculations based on analytical models of pyrazine, if not stated otherwise, 16 384 trajectories were propagated for a total time $t_{\text{max}} = 600$ fs with the time step $\Delta t = 0.1$ fs. (In TRSE calculations, the delay time τ must be added to t_{max} to obtain the total time of the simulation.) In *ab initio* calculations, 256 trajectories were propagated for a total time $t_{\text{max}} = 120$ fs.

E. Methods and software

All quantum calculations were performed using the second-order split-operator algorithm.[81] The LMFD and FSSH dynamics were implemented using the corresponding second-order symplectic Verlet integrator.[82] The Schrödinger equation for the collective discrete electronic degree of freedom was solved using the unitary propagator $\mathbf{U}_{\mathbf{H}_{\text{W}}[X(t)]}(\Delta t) = e^{-i\mathbf{H}_{\text{W}}[X(t)]\Delta t/\hbar}$ evaluated using the package expokit.[83] *Ab initio* electronic structure calculations were performed using Molpro 2010.1 implementation of the CASSCF method.[84]

V. MSDR CALCULATION OF PYRAZINE SPECTRA

The suitability of MSDR for spectra calculations is tested here using three different models of pyrazine: (i) a 4D three-surface model, which allows for comparison with a numerically exact quantum benchmark; (ii) a 24D three-surface model, which explicitly includes all internal degrees of freedom of pyrazine; and (iii) a 30D four-surface *ab initio* model with the electronic structure computed on the fly using the SA-4-CASSCF(10,8)/6-31G* method.

In all calculations, the initial state is the vibrational ground state of the ground PES. Condon approximation is assumed for the transition dipole moment, the only nonzero elements of which are the mutually orthogonal components $\vec{\mu}_{01}$ and $\vec{\mu}_{02}$. Thus, the absorption spectrum reflects the excitation of the molecule either to S_1, S_2, or both, depending on the orientation of the molecule. The TRSE spectra reflect a process in which the pump pulse first excites the initial state to S_1, S_2, or both, and—after free evolution for a delay time τ—the probe pulse of the same polarization brings the resulting density, now spread over S_1 and S_2 surfaces, back to the ground electronic state. For simplicity, we assume that for the pump pulse, the factor $\tilde{E}(\omega_{kl})$ relating components of $\hat{\mu}^{\text{pu}}_{\text{RC,kl}}$ to $\hat{\mu}^{\text{pu}}_{kl}$ via Eq. (20) is constant, $\tilde{E}^{\text{pu}}(\omega_{kl}) \approx \tilde{E}^{\text{pu}}(\omega_c)$, for all transitions of interest (ω_{01}, ω_{02}, ω_{10}, ω_{20}) and is zero for all other transitions,[85] so that the shape of the TRSE spectrum is

This article is copyrighted as indicated in the article. Reuse of AIP content is subject to the terms at: http://scitation.aip.org/termsconditions. Downloaded to IP: 128.178.54.130 On: Fri, 03 Oct 2014 12:49:48

independent of the pump and probe pulses. Within the USP approximation, this is achieved exactly if $\tilde{E}^{\mathrm{pu}}(\omega)$, the Fourier transform of $E^{\mathrm{pu}}(t)$, is a simple step function

$$\begin{aligned} \tilde{E}^{\mathrm{pu}}(\omega) &= \mathrm{const.} = \tilde{E}^{\mathrm{pu}}(\omega_c) \in \mathbb{R} \quad \text{for } \omega \in B, \\ \tilde{E}(\omega) &= 0 \quad \text{for } \omega \notin B, \end{aligned} \tag{55}$$

where $B := [-\omega_{\max}, -\omega_{\min}] \cup [\omega_{\min}, \omega_{\max}]$ is the spectral band of the pulse containing only the frequencies $\pm\omega_{01}$ and $\pm\omega_{02}$ of electronic transitions of interest, and $\omega_{\min} := \omega_c - \Delta\omega/2$ and $\omega_{\max} := \omega_c + \Delta\omega/2$. In the time domain, such a pulse corresponds to a sinc function centered at time 0. For other pulse shapes (such as Gaussian) whose Fourier transform is peaked at ω_c and mostly contained within B, the condition $\tilde{E}^{\mathrm{pu}}(\omega_{kl}) \approx \tilde{E}^{\mathrm{pu}}(\omega_c)$ is satisfied approximately if only the electronic transitions of interest lie within B, and moreover, all these transitions are very close to ω_c.

Due to the accuracy of the rotating wave approximation, the emission term [the second term in Eq. (8)] is neglected in absorption spectra. The transient absorption and bleach contributions to pump-probe spectra are not computed since our focus is specifically the TRSE contribution. Nevertheless, the other terms can be computed easily; e.g., the bleach contribution is, under our assumptions, nothing but a scaled linear absorption spectrum.

In the figures presented below, results obtained with different methods are distinguished by the color of the lines (quantum = green, MSDR_0 = red, MSDR_μ = blue, experiment = black), whereas the line type denotes the underlying dynamics (FSSH = solid, LMFD = dashed). Finally, thickness of lines distinguishes nonadiabatically coupled (thick lines) from corresponding uncoupled (thin lines) systems, in which the nonadiabatic coupling is ignored.

A. Comparison of the MSDR with quantum dynamics using a four-dimensional three-surface model of pyrazine

The four-dimensional three-surface model of pyrazine ("4D model" for short)[49,51] is formulated in the diabatic basis and is based on the quadratic expansion of PESs, linear nonadiabatic coupling between S_1 and S_2, and constant transition dipole moments. Most parameters were taken using the four most important degrees of freedom (including the nonadiabatic coupling mode ν_{10a}) of a 7D model of Ref. 51 except for the energy levels and coupling between states S_1 and S_2 which were taken from Ref. 49. To account for the remaining degrees of freedom and for the environment, a relatively strong phenomenological decay must be introduced into the correlation function. Figure 1(a) shows that the MSDR agrees reasonably well with the quantum result, even though the MSDR spectrum is less resolved, especially in the S_1 region. As is clear from the figure, it is not possible to match the experiment with the 4D model with a single damping time τ_{damp}, even if exact quantum dynamics is used for propagation. With the damping time $\tau_{\mathrm{damp}} = 20$ fs chosen here (for details see Subsection IV B), the S_2 part of the spectrum is reproduced very well, whereas the S_1 part is too broad and too intense. (Incidentally, the S_1 region was not shown in most previous publications that obtained a favorable agreement in the S_2 region.)

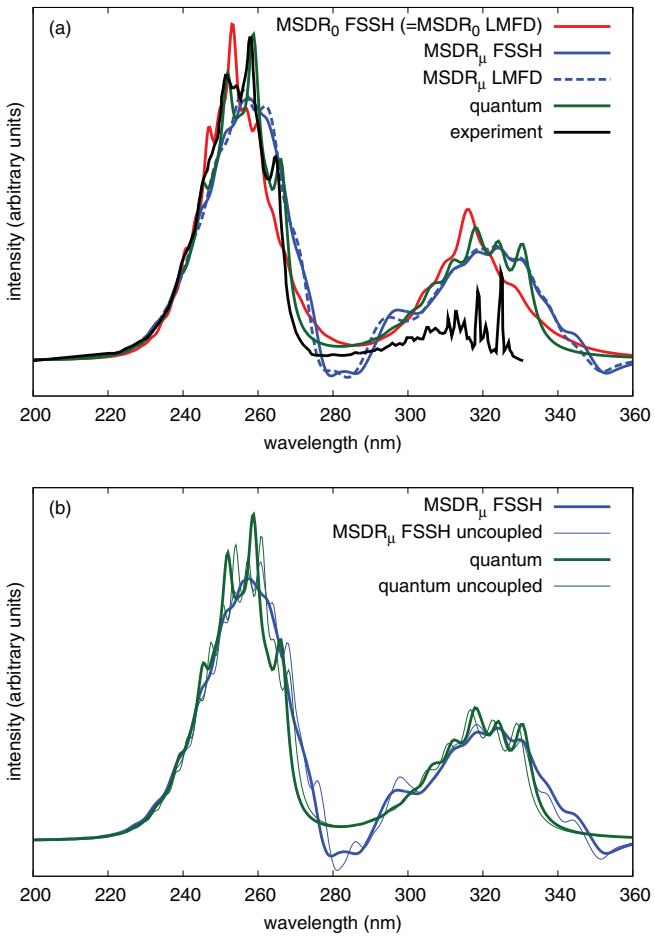

FIG. 1. Absorption spectrum of the 4D model of pyrazine. (a) Comparison of the numerically exact quantum and approximate MSDR spectra of the 4D model with the experimental spectrum. When the nuclear dynamics on the ground surface is employed (MSDR_0), the FSSH dynamics is identical to both LMFD and Born-Oppenheimer dynamics (due to lack of nonadiabatic couplings to the ground surface in the 4D model). When the nuclear dynamics of the excited state is employed (MSDR_μ), the FSSH and LMFD results are not identical, but still very similar. (b) Effect of nonadiabatic couplings on the spectrum. Direction of the spectrum shift due to nonadiabatic couplings is reproduced by the MSDR although its extent is smaller than the true quantum shift.

Figure 1(b) demonstrates the impact of nonadiabatic couplings on the absorption spectra, the most significant effect being the larger separation of the S_1 and S_2 peaks—note that this quantum effect is reproduced qualitatively by the MSDR.

The nonadiabatic effects are much stronger in the TRSE spectrum (see Fig. 2), and the MSDR reproduces the resulting shifts as well as changes in the intensity rather well. Moreover, the FSSH dynamics reproduces better the positive part of the spectrum, whereas the LMFD outperforms the FSSH in the negative feature of the spectrum. In contrast, in the uncoupled system, the rather strong negative feature is qualitatively reproduced even by the FSSH version of the MSDR. [Note that in all figures of TRSE spectra we follow a convention in which the TRSE spectra have an opposite sign to that in Eq. (17).]

This article is copyrighted as indicated in the article. Reuse of AIP content is subject to the terms at: http://scitation.aip.org/termsconditions. Downloaded to IP: 128.178.54.130 On: Fri, 03 Oct 2014 12:49:48

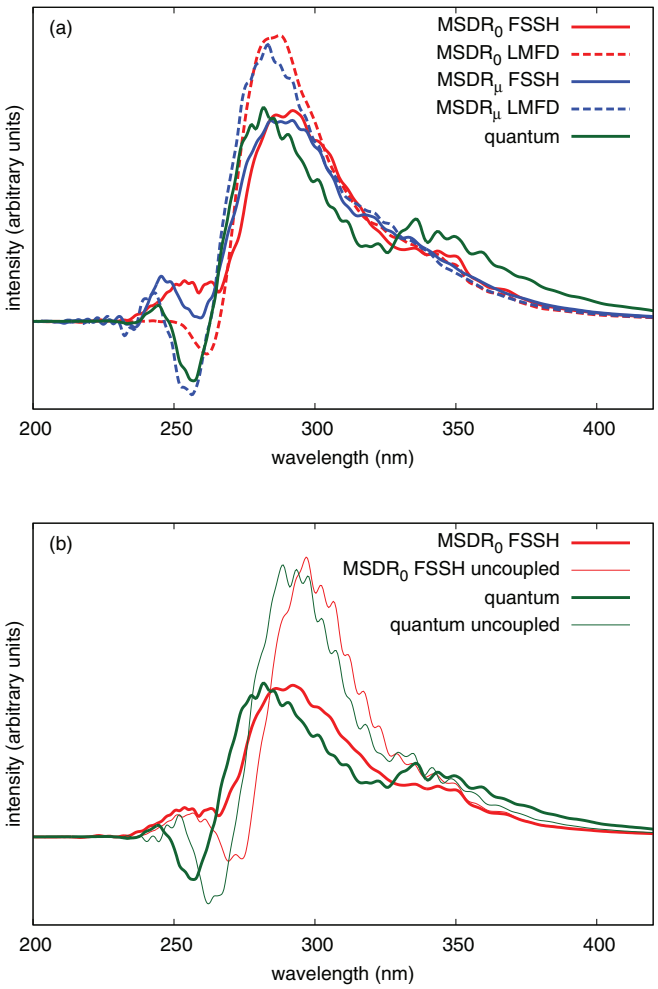

FIG. 2. Time-resolved stimulated emission spectrum of the 4D model of pyrazine at a delay time of 20 fs. (a) Comparison of the approximate MSDR spectra with the numerically exact quantum spectrum. (b) Effect of nonadiabatic couplings on the spectrum. The overall shape of the spectrum as well as shift and decay of intensity due to nonadiabatic couplings are qualitatively reproduced by the MSDR. Note that in contrast to the absorption spectra, MSDR$_0$ here corresponds to the excited state dynamics. In the uncoupled system, the underlying FSSH dynamics propagates each trajectory with the Born-Oppenheimer dynamics on one of the excited states (since no hops are allowed). Following convention, the TRSE spectrum is displayed with a positive sign instead of negative sign present in the general expression given in Eq. (17).

B. MSDR calculations using a 24-dimensional three-surface diabatic model of pyrazine

The more realistic 24-dimensional three-surface diabatic model of pyrazine ("24D model" hereinafter) was taken from Ref. 53. The transition dipole moments as well as the energy difference between the S_2 and ground states, unspecified in Ref. 53, were set to the same values as in the 4D model. The fixed-grid based methods for solving the Schrödinger equation are impracticable in such high-dimensional systems even though other quantum methods such as multi-configuration time-dependent Hartree,[53] full multiple spawning,[56,86] matching-pursuit/split-operator-Fourier-transform,[59] or Gaussian-based multi-configuration time-dependent Hartree[87,88] methods can still be used. Figure 3 shows that the MSDR spectra do not differ much from those

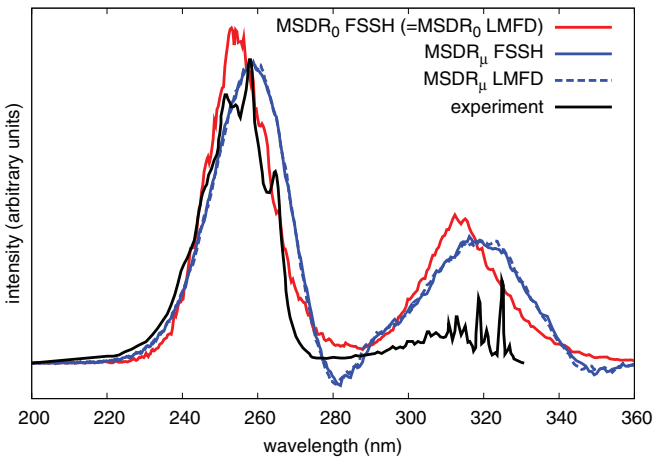

FIG. 3. Absorption spectrum of the 24D model of pyrazine: The envelope is reproduced but the details are lost in the MSDR spectra.

obtained with the 4D model except that they are even less resolved. This happens notwithstanding that a much weaker damping $\tau_{\text{damp}} = 150$ fs was used (the same as in Ref. 53). Indeed, the additional 20 degrees of freedom play a role of explicit environment and cause the broadening of the peaks due to the four most important modes. Still, the lower resolution in comparison with the 4D model is mainly due to the intrinsic error of the MSDR approximation in the additional 20 degrees of freedom, resulting in an artificial decay of the correlation function at later times. Incidentally, this error is aggravated by the fact that the PESs are quadratic and in many degrees of freedom differ only by the force constant. Although the DR is exact in displaced harmonic potentials,[11] and both DR and MSDR usually work well in chaotic systems,[8,26] the nondisplaced harmonic oscillators with changed force constants, despite the apparent simplicity, represent the worst case scenario for both approximations [compare panels (c) and (d) of Fig. 4 in Ref. 25].

Figure 4 compares TRSE spectra computed with and without nonadiabatic couplings, showing that the most important effect of nonadiabatic couplings is a gradual decay of the intensity with the delay time τ. The decay of the TRSE signal integrated over all frequencies agrees quite well with the decay of the averaged population of S_2 (see Fig. 5). The agreement is not prefect due to following facts: First, S_1 also contributes to the signal, although ∼nine times less than S_2; and second, averaging of the populations over orientations does not correspond to the real influence of populations on the spectrum since the states are bright or dark depending on the orientation of the molecule. Still, Fig. 5 clearly demonstrates that in this particular case, the integrated TRSE signal is a good probe of the excited-state population dynamics.

C. MSDR calculations using a 30-dimensional four-surface on-the-fly *ab initio* model of pyrazine

Finally, the MSDR was applied to the 30-dimensional four-surface *ab initio* model of pyrazine based on the state-averaged complete active space self-consistent field [SA-4-CASSCF(10,8)/6-31G*] electronic structure method.[89–91] At

This article is copyrighted as indicated in the article. Reuse of AIP content is subject to the terms at: http://scitation.aip.org/termsconditions. Downloaded to IP: 128.178.54.130 On: Fri, 03 Oct 2014 12:49:48

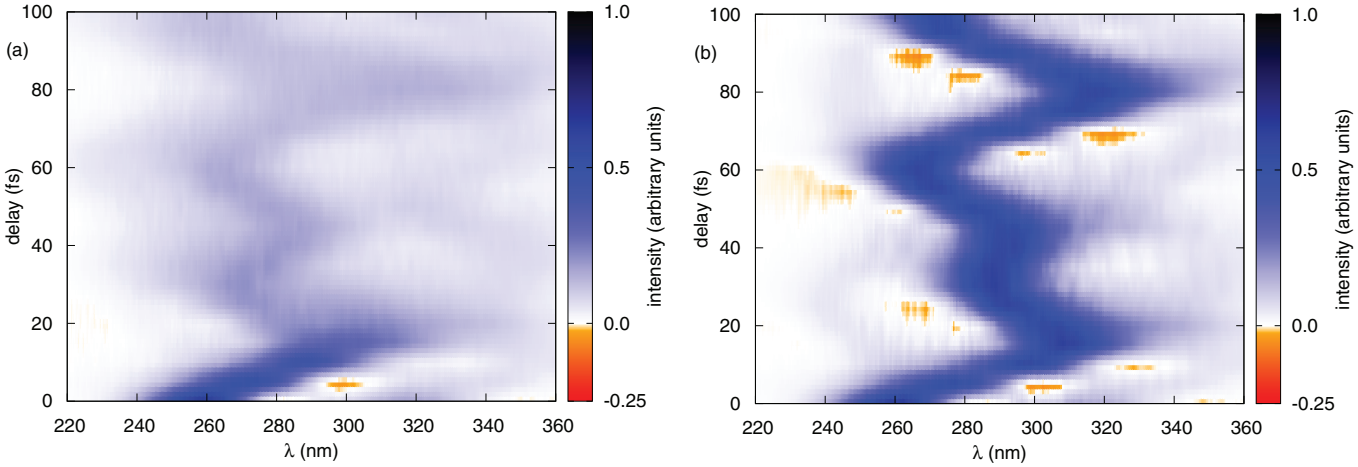

FIG. 4. Time-resolved stimulated emission spectrum of the 24D model of pyrazine. (a) Decay of the TRSE signal with the delay time τ due to nonadiabatic couplings computed with the $MSDR_0$ method and FSSH dynamics. (b) Neglecting the nonadiabatic couplings, the TRSE signal does not decay. Note that if the $MSDR_0$ variant of MSDR is used, the whole time-resolved spectrum can be obtained from a single FSSH simulation of the excited-state dynamics (apart from averaging over orientations of the molecule).

this level of theory, the vertical excitation energies of the three singlet excited states S_1 (corresponding to the $^1B_{3u}$ state), S_2 ($^1B_{2u}$), and S_3 (^1A_u) are 4.85, 5.08, and 5.95 eV, respectively. In comparison with experimental values of 4.04 eV for S_1 and 4.89 eV for S_2 used in the 24D model, the *ab initio* S_2 state lies 0.19 eV higher in energy and the S_1-S_2 gap is reduced substantially. The magnitudes of transition dipole moments of states S_1, S_2, and S_3 to the ground state S_0 are 0.56, 0.36, and 0.0 a.u. Thus, S_3 is a dark state (which, according to more accurate electronic structure calculations, actually has a lower energy than S_2)[61,62] and does not directly influence the calculation—it serves mainly as a stabilizing element in the state-averaged CASSCF calculation.

Due to computational costs of the *ab initio* model the averaging over orientations of pyrazine was not performed. Instead, as the authors of most other published pyrazine calculations, we considered a linearly polarized light and the pyrazine molecule oriented in a way that only the S_2 state is excited. The resulting MSDR absorption spectrum is shown in Fig. 6. Since the shape of the S_2 band is almost unaffected by the intensity borrowing from S_1, the spectrum of the S_2 band can still be compared with the experimental result obtained in the gas phase and hence automatically averaged over orientations. Computed spectra were shifted in energy by 0.19 a.u. to compensate for the inaccuracy of the CASSCF excitation energy, while a phenomenological damping time $\tau = 150$ fs was used to account for the environment as in the 24D model. After the energy shift, the *ab initio* MSDR spectrum reproduces the envelope of the experimental spectrum reasonably well even though it is slightly narrower. In addition, the *ab initio* spectrum oscillates less than the spectrum of the 24D

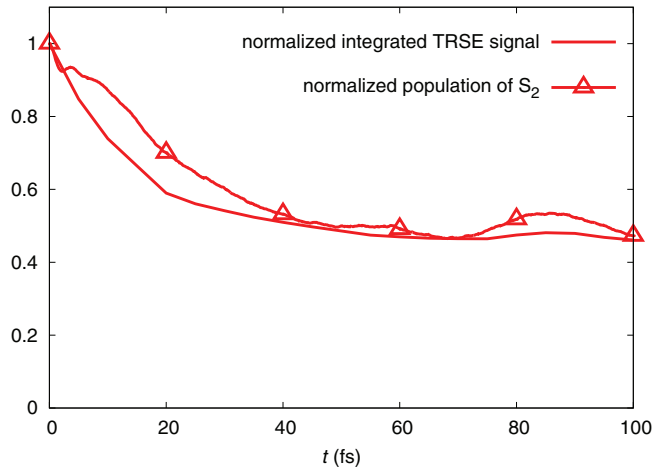

FIG. 5. Time-resolved stimulated emission in the 24D pyrazine model. Comparison of the decay of the integrated intensity of the TRSE spectrum with the decay of the population of the S_2 state after the excitation by the pump pulse (not taking the probe pulse into account). Both quantities are normalized and averaged over orientations of the pyrazine molecule. The result shows that in the isotropic samples of pyrazine the integrated TRSE signal is a good probe of the decay of S_2 population.

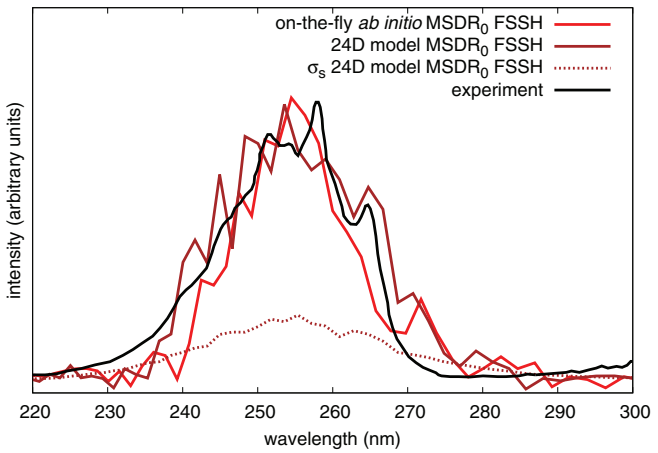

FIG. 6. Absorption spectrum of pyrazine: Comparison of the on-the-fly *ab initio* MSDR spectrum with the MSDR spectrum of the 24D model and with the experimental spectrum. The root mean square statistical error of the spectrum $\sigma_s(N, \lambda)$ was computed for the 24D model following the methodology described in Subsection V D (for $N = 256$). Both MSDR calculations used the FSSH dynamics, 256 trajectories, and the total simulation time $t_{max} = 120$ fs.

This article is copyrighted as indicated in the article. Reuse of AIP content is subject to the terms at: http://scitation.aip.org/termsconditions. Downloaded to IP: 128.178.54.130 On: Fri, 03 Oct 2014 12:49:48

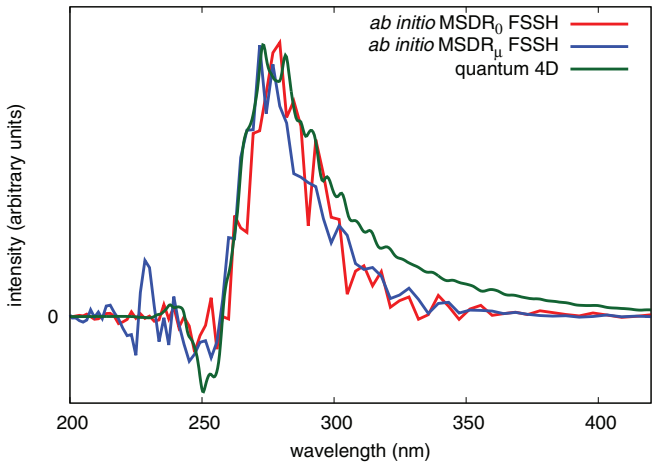

FIG. 7. Time-resolved stimulated emission spectrum of pyrazine at a delay time of 20 fs: Comparison of on-the-fly *ab initio* MSDR spectra with the quantum spectrum of the 4D model. Both MSDR calculations used the FSSH dynamics, 256 trajectories, and total simulation time $t_{\max} = 140$ fs.

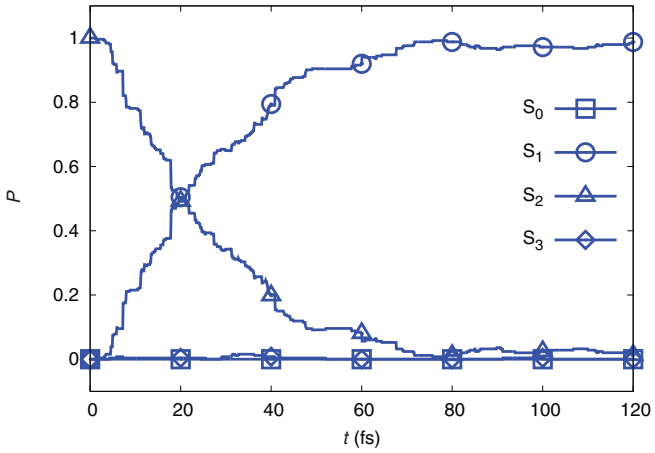

FIG. 8. Populations of the four lowest electronic states of pyrazine obtained with the on-the-fly *ab initio* FSSH dynamics underlying the MSDR$_\mu$ calculation. The molecule of pyrazine is oriented in such a way that only S_2 is initially excited by the pump pulse; the probe pulse is not taken into account. Following the excitation, S_2 decays to S_1 with a half-life of ∼20 fs.

model obtained under the same conditions. Nevertheless, assuming that the statistical error of *ab initio* spectrum is similar to the statistical error $\sigma_s(N, \lambda)$ of the spectrum of the 24D model (see Fig. 6), the "detailed features" of the MSDR spectra should be considered statistical artifacts.

The TRSE spectra of the S_2 state computed with the on-the-fly *ab initio* MSDR are shown in Fig. 7. The MSDR$_0$ and MSDR$_\mu$ agree rather well not only with each other but also with the quantum spectrum of the 4D model with the initial state derived from the CASSCF ground state (instead of the MP2 based ground state used in Ref. 51 and Subsection V A). With this ground state the whole 4D model except for the vertical energies becomes CASSCF based. The comparison with the *ab initio* spectra is thus sensible and suggests that neither the remaining 20 degrees of freedom nor the anharmonicity of S_2 plays a very important role in the TRSE spectra of pyrazine. Note that—in contrast to the coupled 4D model—the MSDR with the FSSH dynamics now seems capable of reproducing the negative feature of the spectrum although barely beyond statistical fluctuations.

The excited-state populations shown in Fig. 8 are obtained from the FSSH excited-state dynamics underlying the MSDR$_\mu$ calculation of absorption spectra (or, equivalently, MSDR$_0$ calculation of the TRSE spectra). The S_2 state decays into S_1 with a half-life of ∼20 fs in an excellent agreement with experimental observations[46] and theoretical calculations based on the TD-DFT method.[92] However, the comparison of Figs. 5 and 8 reveals that the decay is different in the diabatic 24D model and adiabatic *ab initio* model. In the two models, the populations of S_2 decay on a similar time scale but reach different final values after 100 fs. In the diabatic 24D model, the final population is ∼0.4 whereas in the *ab initio* model the population decays nearly to zero. Since the final population is only weakly affected by the averaging procedure used in Fig. 5, the difference between the final population in the two models is probably due to the difference in the model potentials and due to the well-known deficiencies of the FSSH dynamics, namely, the "overcoherence" and the inconsistency between the propagation in the adiabatic and diabatic basis.[69,93,94] Reassuringly, the effect of such differences on spectra is quite weak (see Fig. 6).

D. Statistical convergence of the MSDR

In contrast to the DR,[29] an analytical formula for the statistical error of the MSDR is not available. Nevertheless, it is reasonable to expect that the MSDR inherits some favorable convergence properties from its adiabatic predecessor, most notably the independence of the expected statistical error of the number of degrees of freedom.[29] To test this surmise, we have compared numerically computed statistical errors of the dipole autocorrelation functions in the 4D and 24D models with the analytically evaluated expected statistical error which the DR would attain for the same autocorrelation function.

For the purpose of comparison, we define the root mean square statistical error $\sigma_C(N, t)$ of the normalized dipole autocorrelation function $C_{\mu,n}(N, t) := C_\mu(N, t)/C_\mu(N, 0)$ as

$$\sigma_C(N,t)^2 = \overline{\left|C_{\mu,n}(N,t) - C_{\mu,n}(\infty,t)\right|^2}, \qquad (56)$$

where the overline denotes an average over an infinite number of simulations with different sets of N trajectories. Not having an infinite number of simulations at hand, the errors were estimated numerically using 100 independent simulations, each with $N = 4096$ trajectories. To project out the effect of the actual number of trajectories used, $\sigma_C(4096, t)$ were converted into an error per trajectory $\sigma_C(1, t) := N^{1/2}\sigma_C(N, t)$.

The results are shown in Fig. 9. Whereas both the 4D and 24D models exhibit the same initial decay of $|C_{\mu,n}|$, the recurrences present in the 4D model are suppressed in the 24D model. Yet, the statistical error σ_C of the MSDR appears to be independent of the dimensionality. Moreover, within the statistical error of σ_C itself, the MSDR error $\sigma_{C,\mathrm{MSDR}}$ is the same as the error $\sigma_{C,\mathrm{DR}}$ of the DR, captured by the analytical formula $\sigma_{C,\mathrm{DR}}(1, t)^2 = 1 - |C_{\mu,n}(\infty, t)|^2$.

This article is copyrighted as indicated in the article. Reuse of AIP content is subject to the terms at: http://scitation.aip.org/termsconditions. Downloaded to IP: 128.178.54.130 On: Fri, 03 Oct 2014 12:49:48

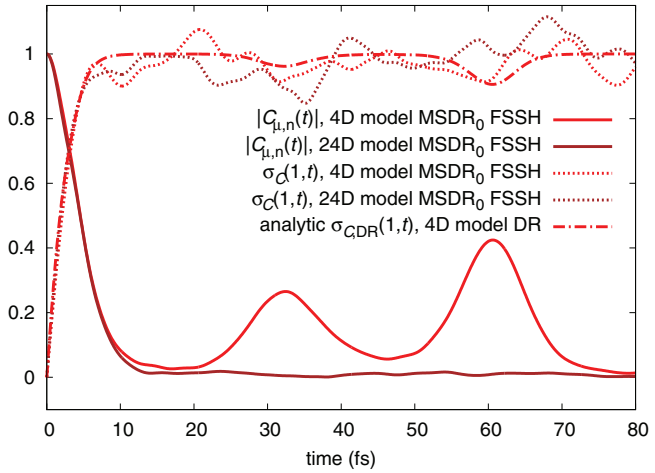

FIG. 9. Statistical errors: Comparison of normalized dipole autocorrelation functions $|C_{\mu,n}|$ and root mean square errors of $C_{\mu,n}$ per trajectory $[\sigma_C(1,t)]$ for the MSDR calculations in the 4D and 24D models. The analytically computed error $\sigma_{C,\mathrm{DR}}(1,t)$ shows the hypothetical statistical error of $C_{\mu,n}$ if it were computed with the DR instead of MSDR. Whereas the recurrences of the correlation function $|C_{\mu,n}|$ are much weaker in the 24D model than in 4D model, the statistical error $\sigma_C(1,t)$ of the MSDR appears to be independent of dimensionality. In addition—within statistical fluctuations due to the finite number of simulations—this error agrees with $\sigma_{C,\mathrm{DR}}(1,t)$.

VI. CONCLUSION

We have extended the MSDR method in order that it can be used to evaluate correlation functions needed for the calculations of linear and pump-probe spectra involving nonadiabatic effects. By computing the absorption and TRSE spectra of pyrazine, we have shown that the MSDR captures qualitatively the main features of the spectra. However, since the MSDR cannot accurately resolve vibrational peaks, it is less suitable for calculations of absorption spectra unless one is primarily interested in the envelope of the spectrum or the qualitative effect of nonadiabatic couplings. On the other hand, our calculations confirm the utility of the MSDR for the evaluation of TRSE spectra, where the main features (i.e., decay of intensity due to nonadiabatic coupling, shifts of the maxima as a function of delay time, and negative features) are often the only features of interest to experimentalists and are all described rather well with the method.

Although MSDR may be less accurate than other semiclassical or mixed quantum-classical methods for computing nonadiabatic electronic spectra, the main practical advantages of the MSDR are its efficiency and simplicity—in contrast to approaches[31] based on the semiclassical initial value representation, the MSDR does not require the Hessian of the potential energy, and, unlike methods[79] directly solving the MQCL equation, the MSDR relies on dynamical equations that are easy to solve numerically. In particular, in MSDR each trajectory carries all components of the density matrix, whereas in direct solutions of the MQCL equation, each component of the density matrix is propagated with a separate ensemble of trajectories. In this sense, MSDR is related to an approximate solution of the MQCL equation proposed by Roman and Martens,[78] in which the full density matrix is propagated using a single ensemble of trajectories, evolved with a reference Hamiltonian and yielding accurate results at lower costs than direct solutions of the MQCL equation. However, unlike the method of Roman and Martens[78] and direct approaches to solve the MQCL equation, where different trajectories within an ensemble feel the same Hamiltonian, in MSDR each trajectory feels its own locally mean-field Hamiltonian (in MSDR/LMFD) or instantaneous Born-Oppenheimer Hamiltonian (in MSDR/FSSH); this does not cause numerical difficulties since MSDR trajectories do not communicate.

As the computational cost per trajectory of the MSDR exceeds only very slightly the cost of the FSSH or Ehrenfest dynamics, our method can be readily applied on the fly. In addition, the implementation of the MSDR into a code for FSSH or Ehrenfest dynamics is very simple; essentially, apart from the computation of the dipole operator matrix, only four additional operations are needed: (i) For each trajectory, one must perform an additional propagation of the electronic degree of freedom (using the same Hamiltonian matrix as for the LMFD or FSSH dynamics but with a different initial condition). (ii) One must compute the overlap of the two electronic states resulting from the two propagations. This amounts to a dot product of vectors for pure states, or to a trace of a matrix product for general states at each step and for each trajectory. (iii) The dipole autocorrelation function is computed at every step as an average of this overlap over all trajectories. (iv) At the end of simulation, the spectrum is obtained as the Fourier transform of the dipole autocorrelation function.

The approximate MSDR dynamics underlying both the absorption and TRSE spectra is the dynamics on either the ground or excited surface; both absorption and TRSE spectra can therefore be computed almost for free during a standard excited-state calculation.

In the future, the effects of using the non-Condon dipole operator and propagation of the nuclei according to the average electronic density should be explored. In addition, the MSDR may be generalized in a relatively straightforward way to compute different autocorrelation functions. Also, a possibility of adding a decoherence correction[93,94] to the underlying FSSH dynamics may be considered. Finally, the accuracy and efficiency of the method may be improved by implementing a prefactor amplitude correction,[24,25] cellularization,[19,25] or by replacing the trajectories with evolving Gaussian basis functions,[26] i.e., ideas that have been used successfully in the Born-Oppenheimer DR.[19,24–26]

ACKNOWLEDGMENTS

We would like to thank Hans-Dieter Meyer for providing us with the parameter file for the 24D model of pyrazine. This research was supported by the Swiss National Science Foundation (NSF(CH)) within the National Center of Competence in Research "Molecular Ultrafast Science & Technology" (NCCR MUST) and by the EPFL.

APPENDIX: DERIVATION OF EXPRESSIONS RELATING LINEAR AND PUMP-PROBE SPECTRA TO DIPOLE TIME-CORRELATION FUNCTIONS

In this appendix, we provide derivations of perturbative expressions for linear and pump probe spectra in the general

This article is copyrighted as indicated in the article. Reuse of AIP content is subject to the terms at: http://scitation.aip.org/termsconditions. Downloaded to IP: 128.178.54.130 On: Fri, 03 Oct 2014 12:49:48

setting of mixed states, arbitrary couplings between electronic states, and arbitrary pulse shapes.

1. Nonperturbative electric-dipole spectrum

We start by reviewing the relation between the nonperturbative spectrum and polarization of the sample using the density operator formalism; for a detailed derivation in the wavefunction setting, see, e.g., Ref. 95 or Tannor's textbook.[80] In this subsection (only), we consider the exact, nonperturbative density operator $\hat{\boldsymbol{\rho}}_{\text{tot}}(t)$ obtained by evolution with the total Hamiltonian $\hat{\mathbf{H}}_{\text{tot}}(t)$ using the von Neumann equation

$$i\hbar\frac{d}{dt}\hat{\boldsymbol{\rho}}_{\text{tot}}(t) = [\hat{\mathbf{H}}_{\text{tot}}(t), \hat{\boldsymbol{\rho}}_{\text{tot}}(t)]. \tag{A1}$$

In general, spectrum provides a measure of the energy transfer between the electromagnetic field and the molecule. The rate of change of the molecule's energy is simply the time derivative of the expectation value of the total Hamiltonian

$$\frac{d}{dt}H_{\text{tot}} = \frac{d}{dt}\,\text{Tr}[\hat{\boldsymbol{\rho}}_{\text{tot}}(t)\,\hat{\mathbf{H}}_{\text{tot}}(t)] = -\vec{P}(t)\cdot\frac{d}{dt}\vec{E}(t), \tag{A2}$$

where the second equality was obtained using Eq. (A1) and by introducing the polarization

$$\vec{P}(t) := \text{Tr}(\hat{\boldsymbol{\rho}}_{\text{tot}}(t)\,\hat{\vec{\boldsymbol{\mu}}}) \tag{A3}$$

as the expectation value of the electric dipole operator. The total energy transferred is obtained by integrating Eq. (A2) over all times

$$\begin{aligned}\Delta H_{\text{tot}} &= -\int_{-\infty}^{\infty}\vec{P}(t)\cdot\frac{d}{dt}\vec{E}(t)\,dt\\ &= 2\pi i\int_{-\infty}^{\infty}\omega\,\tilde{\vec{P}}(\omega)^*\cdot\tilde{\vec{E}}(\omega)\,d\omega\\ &= \int_{-\infty}^{\infty}\Delta H(\omega)\,d\omega,\end{aligned} \tag{A4}$$

where $\tilde{\vec{E}}(\omega)$ and $\tilde{\vec{P}}(\omega)$ are the Fourier transforms of the polarization and electric field. The second equality follows from the Plancherel theorem and the Fourier-derivative relation, while the third equality introduces the total energy absorbed per unit frequency

$$\Delta H(\omega) := -2\pi\omega\,\text{Im}[\tilde{\vec{P}}(\omega)^*\cdot\tilde{\vec{E}}(\omega)]. \tag{A5}$$

The incident field energy per area ("radiation exposure") is computed by integrating the incident energy flux (i.e., the magnitude of the Poynting vector) $S(t) := c|\vec{E}(t)\times\vec{B}(t)|/(4\pi) = cE(t)^2/(4\pi)$ over all times,

$$\frac{\text{Incident energy}}{\text{Area}} = \int_{-\infty}^{\infty}S(t)\,dt = \frac{c}{2}\int_{-\infty}^{\infty}|\tilde{E}(\omega)|^2\,d\omega, \tag{A6}$$

where the Plancherel theorem was used again.

Now we are ready to define the spectrum as the frequency-dependent cross section for the energy transfer from the field to the molecule

$$\sigma(\omega) := \frac{\text{Energy transferred at }\omega}{\text{Incident energy per area at }\omega} = \frac{\Delta H(\omega)}{c|\tilde{E}(\omega)|^2/2}, \tag{A7}$$

where the denominator is the incident field energy per unit frequency and area, and can be read off from Eq. (A6). Combining Eqs. (A5) and (A7), we arrive at the promised expression connecting the nonperturbative spectrum to the polarization of the sample

$$\sigma(\omega) = \frac{4\pi\omega}{c}\frac{\text{Im}[\tilde{\vec{P}}(\omega)\cdot\tilde{\vec{E}}(\omega)^*]}{|\tilde{E}(\omega)|^2}. \tag{A8}$$

This formula, valid for both continuous-wave and ultrafast experiments with both weak and strong fields, captures absorption and emission spectra, vibronic and rovibrational spectra, as well as linear and nonlinear spectra.

2. Time-dependent perturbation theory for polarization

In a majority of spectroscopic experiments, the fields are relatively weak, and expression (A8) can be expanded in orders of TDPT. Although the TDPT does not necessarily simplify numerical calculations, it often facilitates the interpretation of such spectra.

To compute the spectrum from expression (A8), one needs to find the polarization, which—within the TDPT—may be expanded in a series[63]

$$\vec{P}_{\text{tot}}(t) \sim \sum_{n=0}^{\infty}\vec{P}^{(n)}(t), \tag{A9}$$

where the nth-order polarization depends on the nth power of the electric field and is obtained as

$$\vec{P}^{(n)}(t) := \text{Tr}[\hat{\boldsymbol{\rho}}^{(n)}(t)\,\hat{\vec{\boldsymbol{\mu}}}] \tag{A10}$$

from the corresponding term of the perturbative expansion of the density operator

$$\hat{\boldsymbol{\rho}}_{\text{tot}}(t) \sim \sum_{n=0}^{\infty}\hat{\boldsymbol{\rho}}^{(n)}(t). \tag{A11}$$

The nth-order term of the density operator is conveniently expressed in the interaction picture,

$$\hat{\boldsymbol{\rho}}_I^{(n)}(t) := \hat{\mathbf{U}}(t)^\dagger\hat{\boldsymbol{\rho}}^{(n)}(t)\hat{\mathbf{U}}(t), \tag{A12}$$

in which it is given by

$$\begin{aligned}\hat{\boldsymbol{\rho}}_I^{(n)}(t) = \left(\frac{i}{\hbar}\right)^n\int_{-\infty}^{t}dt_n\int_{-\infty}^{t_n}dt_{n-1}\cdots\int_{-\infty}^{t_2}dt_1\\ \times[\vec{E}(t_n)\cdot\hat{\vec{\boldsymbol{\mu}}}(t_n),[\cdots[\vec{E}(t_1)\cdot\hat{\vec{\boldsymbol{\mu}}}(t_1),\hat{\boldsymbol{\rho}}]\cdots]],\end{aligned} \tag{A13}$$

where we have used the stationarity (10) of $\hat{\boldsymbol{\rho}}$.

3. Linear electric-dipole spectrum

Let us denote the projection of the molecular polarization onto the polarization of the laser field by $P(t) := \vec{P}(t)\cdot\vec{\epsilon}$. The linear electric-dipole spectrum is obtained[63] simply by substituting into the general nonperturbative expression (A8) the

This article is copyrighted as indicated in the article. Reuse of AIP content is subject to the terms at: http://scitation.aip.org/termsconditions. Downloaded to IP: 128.178.54.130 On: Fri, 03 Oct 2014 12:49:48

linear polarization

$$P^{(1)}(t) = \mathrm{Tr}[\hat{\boldsymbol{\rho}}^{(1)}(t)\hat{\boldsymbol{\mu}}] = \mathrm{Tr}\left[\hat{\boldsymbol{\rho}}_I^{(1)}(t)\hat{\boldsymbol{\mu}}(t)\right] = \frac{i}{\hbar}\int_{-\infty}^{t} dt_1 E(t_1)\,\mathrm{Tr}\{[\hat{\boldsymbol{\mu}}(t_1), \hat{\boldsymbol{\rho}}]\hat{\boldsymbol{\mu}}(t)\}. \quad \text{(A14)}$$

By noting that

$$\mathrm{Tr}\{[\hat{\boldsymbol{\mu}}(t_1), \hat{\boldsymbol{\rho}}]\hat{\boldsymbol{\mu}}(t)\} = \mathrm{Tr}\{[\hat{\boldsymbol{\mu}}, \hat{\boldsymbol{\rho}}(t_1)]\hat{\boldsymbol{\mu}}(t-t_1)\} = \mathrm{Tr}\{[\hat{\boldsymbol{\mu}}, \hat{\boldsymbol{\rho}}]\hat{\boldsymbol{\mu}}(t-t_1)\}, \quad \text{(A15)}$$

which follows from the cyclic property of the trace and stationarity (10) of $\hat{\boldsymbol{\rho}}$, and by changing variables to $t' := t - t_1$, one can rewrite the linear polarization (A14) as

$$P^{(1)}(t) = \frac{i}{\hbar}\int_0^{\infty} dt' E(t-t')[C_\mu^{(1)}(t')^* - C_\mu^{(1)}(t')], \quad \text{(A16)}$$

where $C_\mu^{(1)}(t) := \mathrm{Tr}[\hat{\boldsymbol{\rho}}\,\hat{\boldsymbol{\mu}}\,\hat{\boldsymbol{\mu}}(t)] = \mathrm{Tr}[\hat{\boldsymbol{\rho}}\,\hat{\boldsymbol{\mu}}(t)\hat{\boldsymbol{\mu}}]^*$ is the dipole time-autocorrelation function (9), the second equality following from the cyclic property of the trace and hermiticity of $\hat{\boldsymbol{\mu}}$ and $\hat{\boldsymbol{\rho}}$. Using the causal form of the correlation function

$$S_\mu^{(1)}(t) := \theta(t) C_\mu^{(1)}(t),$$

where θ is the Heaviside function [$\theta(t) = 1$ for $t \geq 0$ and $\theta(t) = 0$ for $t < 0$], one can express the polarization as

$$P^{(1)} = \frac{i}{\hbar} E * \left(S_\mu^{(1)*} - S_\mu^{(1)}\right), \quad \text{(A17)}$$

where $*$ denotes the convolution

$$(f * g)(t) := \int_{-\infty}^{\infty} f(t-t')g(t')dt'. \quad \text{(A18)}$$

Substitution of the Fourier-transformed polarization,

$$\tilde{P}^{(1)} = \frac{2\pi i}{\hbar}\tilde{E}\left(\widetilde{S_\mu^{(1)*}} - \widetilde{S_\mu^{(1)}}\right), \quad \text{(A19)}$$

obtained from Eq. (A17) using the convolution theorem, into the nonperturbative expression (A8) completes the derivation of the linear spectrum (8).

4. Pump-probe electric-dipole spectrum

Assuming nonparallel pump and probe laser beams and heterodyne detection in the direction $\vec{k}^{\mathrm{pr}}$ of the probe beam,[6] the cross section $\sigma(\omega, \tau)$ [Eq. (16)] corresponding to the differential pump-probe spectrum is found by subtracting the cross section for the probe only [$\sigma^{\mathrm{pr}}(\omega)$] from the cross section for both pulses combined [$\sigma^{\mathrm{pu+pr}}(\omega, \tau)$]. The differential spectrum is therefore obtained by substituting the differential polarization $\delta\vec{P} := \vec{P}^{\mathrm{pu+pr}}_{\vec{k}^{\mathrm{pr}}} - \vec{P}^{\mathrm{pr}}_{\vec{k}^{\mathrm{pr}}}$, where $\vec{P}^{j}_{\vec{k}^{\mathrm{pr}}}$ is the component of the total polarization $\vec{P}^{j}$ in experiment j radiating in the direction $\vec{k}^{\mathrm{pr}}$, into the general nonperturbative expression (A8)[96]

$$\sigma(\omega, \tau) = \frac{4\pi\omega}{c}\frac{\mathrm{Im}[\delta\tilde{\vec{P}}(\omega, \tau)\cdot\widetilde{\vec{E}^{\mathrm{pr}}}(\omega)^*]}{|\tilde{E}^{\mathrm{pr}}(\omega)|^2}. \quad \text{(A20)}$$

Using the TDPT, the leading term of the differential polarization $\delta\vec{P}$ is $\delta\vec{P}^{(3)}$ since the first-order terms $\vec{P}^{\mathrm{pu+pr},(1)}_{\vec{k}^{\mathrm{pr}}}$ and $\vec{P}^{\mathrm{pr},(1)}_{\vec{k}^{\mathrm{pr}}}$ cancel each other in the difference $\delta\vec{P}$ and since the second-order polarization $\vec{P}^{j,(2)}$ vanishes in media with inversion symmetry.[6] In analogy to the derivation of nonperturbative spectrum (A8) from the total energy transfer (A4), the third-order pump-probe spectrum (A20) can be derived from the energy transfer

$$\Delta\delta H^{(3)} = -\int_{-\infty}^{\infty} \delta\vec{P}^{(3)}(t)\cdot\frac{d}{dt}\vec{E}^{\mathrm{pr}}(t)\,dt, \quad \text{(A21)}$$

where the total third-order polarization in experiment j is defined as

$$\vec{P}^{j,(3)}(t) = \mathrm{Tr}[\hat{\boldsymbol{\rho}}^{j,(3)}(t)\hat{\vec{\boldsymbol{\mu}}}] = \mathrm{Tr}\left[\hat{\boldsymbol{\rho}}_I^{(3)}(t)\hat{\vec{\boldsymbol{\mu}}}(t)\right], \quad \text{(A22)}$$

in terms of the third-order density operator, given by

$$\hat{\boldsymbol{\rho}}_I^{j,(3)}(t) = \left(\frac{i}{\hbar}\right)^3\int_{-\infty}^{t} dt_3\int_{-\infty}^{t_3} dt_2\int_{-\infty}^{t_2} dt_1 \times [\vec{E}^j(t_3)\cdot\hat{\vec{\boldsymbol{\mu}}}(t_3), [\vec{E}^j(t_2)\cdot\hat{\vec{\boldsymbol{\mu}}}(t_2), \times [\vec{E}^j(t_1)\cdot\hat{\vec{\boldsymbol{\mu}}}(t_1), \hat{\boldsymbol{\rho}}]]]. \quad \text{(A23)}$$

Assuming the widths of the pump and probe pulses to be much smaller than the delay τ, one may make the NOP approximation, which mathematically amounts to computing the differential density $\delta\hat{\boldsymbol{\rho}}_I^{(3)}(t)$ from Eq. (A23) for $\hat{\boldsymbol{\rho}}_I^{j,(3)}(t)$ by replacing $\vec{E}^j$ with $\vec{E}^{\mathrm{pu}}$ at times t_1 and t_2 and with $\vec{E}^{\mathrm{pr}}$ at time t_3, as well as by replacing the upper limit t_3 with ∞ in the integral over t_2. [More generally, the NOP approximation only implies that all interactions with $\vec{E}^{\mathrm{pr}}$ follow all interactions with $\vec{E}^{\mathrm{pu}}$; altogether there are four such terms since the last of the four interactions–the one in Eq. (A21)–is always with $\vec{E}^{\mathrm{pr}}$; however, only the above-mentioned term $(\vec{E}^{\mathrm{pu}})^2(\vec{E}^{\mathrm{pr}})^2$ survives since the terms $\vec{E}^{\mathrm{pu}}(\vec{E}^{\mathrm{pr}})^3$ and $(\vec{E}^{\mathrm{pu}})^3\vec{E}^{\mathrm{pr}}$ with odd interactions with the pump do not propagate in the direction of the probe beam,[6] and $(\vec{E}^{\mathrm{pr}})^4$ vanishes in the differential spectrum since two identical terms of this type cancel each other in the differential polarization $\delta\vec{P}^{(3)} = \vec{P}^{\mathrm{pu+pr},(3)}_{\vec{k}^{\mathrm{pr}}} - \vec{P}^{\mathrm{pr},(3)}_{\vec{k}^{\mathrm{pr}}}$.] Using dipole moment projections (14) and (15), denoting similarly $\delta P^{(3)}(t) := \delta\vec{P}^{(3)}(t)\cdot\vec{\epsilon}^{\mathrm{pr}}$, within the NOP approximation Eqs. (A21)–(A23) for $\Delta H^{(3)}$ simplify to

$$\Delta\delta H^{(3)}_{\mathrm{NOP}} = -\int_{-\infty}^{\infty}\frac{d}{dt}E^{\mathrm{pr}}(t)\delta P^{(3)}_{\mathrm{NOP}}(t)\,dt, \quad \text{(A24)}$$

$$\delta P^{(3)}_{\mathrm{NOP}}(t) = \mathrm{Tr}\left[\delta\hat{\boldsymbol{\rho}}^{(3)}_{I,\mathrm{NOP}}(t)\hat{\boldsymbol{\mu}}^{\mathrm{pr}}(t)\right], \quad \text{(A25)}$$

$$\delta\hat{\boldsymbol{\rho}}^{(3)}_{I,\mathrm{NOP}}(t) = \frac{i}{\hbar}\int_{-\infty}^{t} dt_3\left[E^{\mathrm{pr}}(t_3)\hat{\boldsymbol{\mu}}^{\mathrm{pr}}(t_3), \hat{\boldsymbol{\rho}}^{\mathrm{pu}}_{\mathrm{NOP}}\right], \quad \text{(A26)}$$

where $\hat{\boldsymbol{\rho}}^{\mathrm{pu}}_{\mathrm{NOP}}$ is the second-order density operator generated by the pump pulse,

$$\hat{\boldsymbol{\rho}}^{\mathrm{pu}}_{\mathrm{NOP}} := \left(\frac{i}{\hbar}\right)^2\int_{-\infty}^{\infty} dt_2\int_{-\infty}^{t_2} dt_1 \times [E^{\mathrm{pu}}(t_2)\hat{\boldsymbol{\mu}}^{\mathrm{pu}}(t_2), [E^{\mathrm{pu}}(t_1)\hat{\boldsymbol{\mu}}^{\mathrm{pu}}(t_1), \hat{\boldsymbol{\rho}}]]. \quad \text{(A27)}$$

Note that for nonoverlapping pulses the four-dimensional time integral for $\Delta\delta H^{(3)}$ [Eqs. (A21)–(A23)] decouples into two independent two-dimensional integrals, one for $\Delta\delta H^{(3)}_{\mathrm{NOP}}$ [Eqs. (A24)–(A26)] and one for $\hat{\boldsymbol{\rho}}^{\mathrm{pu}}_{\mathrm{NOP}}$ [Eq. (A27)].

This article is copyrighted as indicated in the article. Reuse of AIP content is subject to the terms at: http://scitation.aip.org/termsconditions. Downloaded to IP: 128.178.54.130 On: Fri, 03 Oct 2014 12:49:48

Within the *ultrashort pulse* (USP or *impulsive*) *approximation* for the pump pulse, the pulse envelope δ_n^{pu} is assumed to be a delta function on the nuclear time scale, so the nuclei do not move during the pump excitation. One often considers a Gaussian δ_n^{pu} with a width much shorter than the vibrational period and much longer than the electronic period, and a harmonic electronic factor $E_e^{\mathrm{pu}}(t) = E_0^{\mathrm{pu}} \cos(\omega_c t - \varphi^{\mathrm{pu}})$. Since the derivation for arbitrary pulse shapes is not difficult, below we will use neither this form nor the splittings (12) and (13) of the electric field into electronic and nuclear factors, and will instead work with general $E^{\mathrm{pu}}(t)$, assuming only that it is localized at time 0 and that the bandwidth of the pulse is narrow on electronic scale and wide on nuclear scale. As a result, the pulse excites only electronic states of interest, but within those states, all vibrational levels are excited equally.

By expanding $E^{\mathrm{pu}}(t) = \int \tilde{E}^{\mathrm{pu}}(\omega) e^{-i\omega t} d\omega$ and using the USP approximation $\hat{\boldsymbol{\mu}}^{\mathrm{pu}}(t) \approx \hat{\boldsymbol{\mu}}^{\mathrm{pu}}_{\mathrm{USP}}(t) := \sum_{kl} \mu^{\mathrm{pu}}_{kl} |k\rangle\langle l| e^{i\omega_{kl} t}$ in Eq. (A27) for $\hat{\boldsymbol{\rho}}^{\mathrm{pu}}_{\mathrm{NOP}}$, where $\hbar\omega_{kl}$ is the difference between the energies of electronic states k and l, one obtains

$$\begin{aligned}
\hat{\boldsymbol{\rho}}^{\mathrm{pu}}_{\mathrm{NOP+USP}} &:= \int_{-\infty}^{\infty} dt_2 \int_{-\infty}^{\infty} d\omega_2 \tilde{E}^{\mathrm{pu}}(\omega_2) \int_{-\infty}^{t_2} dt_1 \int_{-\infty}^{\infty} d\omega_1 \tilde{E}^{\mathrm{pu}}(\omega_1) \\
&\quad \times \sum_{klmn} \hat{\mathbf{C}}_{klmn} \exp[i(\omega_{kl} - \omega_2) t_2 + i(\omega_{mn} - \omega_1) t_1], \\
\hat{\mathbf{C}}_{klmn} &:= \left(\frac{i}{\hbar}\right)^2 \left[\hat{\mu}^{\mathrm{pu}}_{kl} |k\rangle\langle l|, \left[\hat{\mu}^{\mathrm{pu}}_{mn} |m\rangle\langle n|, \hat{\boldsymbol{\rho}}\right]\right].
\end{aligned}$$

By changing variables from t_1 to $t_1' := t_2 - t_1$, one can separate and analytically evaluate the two time integrals,

$$\begin{aligned}
\hat{\boldsymbol{\rho}}^{\mathrm{pu}}_{\mathrm{NOP+USP}} &:= \int_{-\infty}^{\infty} d\omega_2 \tilde{E}^{\mathrm{pu}}(\omega_2) \int_{-\infty}^{\infty} d\omega_1 \tilde{E}^{\mathrm{pu}}(\omega_1) \\
&\quad \times \sum_{klmn} \hat{\mathbf{C}}_{klmn} \int_{-\infty}^{\infty} dt_2 \exp[i(\omega_{kl} \\
&\quad + \omega_{mn} - \omega_1 - \omega_2) t_2] \\
&\quad \times \int_{-\infty}^{\infty} dt_1' \theta(t_1') \exp[i(\omega_1 - \omega_{mn}) t_1'] \\
&= \int_{-\infty}^{\infty} d\omega_2 \tilde{E}^{\mathrm{pu}}(\omega_2) \int_{-\infty}^{\infty} d\omega_1 \tilde{E}^{\mathrm{pu}}(\omega_1) \sum_{klmn} \hat{\mathbf{C}}_{klmn} \\
&\quad \times 2\pi \delta(\omega_{kl} + \omega_{mn} - \omega_1 - \omega_2) \\
&\quad \times \left[\pi \delta(\omega_1 - \omega_{mn}) + \mathcal{PV} \frac{i}{\omega_1 - \omega_{mn}}\right] \\
&\approx 2\pi^2 \sum_{klmn} \tilde{E}^{\mathrm{pu}}(\omega_{kl}) \tilde{E}^{\mathrm{pu}}(\omega_{mn}) \hat{\mathbf{C}}_{klmn} \\
&= 2\pi^2 \hbar^{-2} \left[\hat{\boldsymbol{\mu}}^{\mathrm{pu}}_{\mathrm{RC}}, \left[\hat{\boldsymbol{\rho}}, \hat{\boldsymbol{\mu}}^{\mathrm{pu}}_{\mathrm{RC}}\right]\right] =: \hat{\boldsymbol{\rho}}^{\mathrm{pu}}_{\mathrm{NOP+USP+RC}},
\end{aligned} \tag{A28}$$

where, on the penultimate line, we used the RC to neglect the Cauchy principal value ($\mathcal{PV}$) contribution to the ω_1 integral, and, on the last line, introduced the resonant dipole moment (20).

Since we are interested in the signal in the direction of the probe pulse, the PM implies that the momentum transfer between the molecule and the pump pulse must approximately vanish ($\hbar\vec{k}_1^{\mathrm{pu}} - \hbar\vec{k}_2^{\mathrm{pu}} \approx 0$) and therefore frequencies $\omega_1 (= \omega_{kl})$ and $\omega_2 (= \omega_{mn})$ in the derivation of Eq. (A28) must be approximately equal in magnitude but of opposite sign. Assuming again that the bandwidth of E^{pu} is relatively narrow, i.e., that the pump excites only nearly degenerate electronic transitions, while the detector is sufficiently large to detect signal with a slightly mismatched momentum transfer $\hbar\vec{k}_1^{\mathrm{pu}} - \hbar\vec{k}_2^{\mathrm{pu}}$ corresponding to these two transitions, the PM implies that instead of $\hat{\boldsymbol{\rho}}^{\mathrm{pu}}_{\mathrm{NOP+USP+RC}}$, one should actually use

$$\begin{aligned}
&\hat{\boldsymbol{\rho}}^{\mathrm{pu}}_{\mathrm{NOP+USP+RC+PM}} \\
&\quad := 2\pi^2 \sum_{\substack{klmn \\ \omega_{kl} \approx -\omega_{mn}}} \tilde{E}^{\mathrm{pu}}(\omega_{kl}) \tilde{E}^{\mathrm{pu}}(\omega_{mn}) \hat{\mathbf{C}}_{klmn} \\
&\quad = 2\pi^2 \hbar^{-2} \left(\left[\hat{\boldsymbol{\mu}}^{\mathrm{pu}\dagger}_{\mathrm{RC+PM}}, \left[\hat{\boldsymbol{\rho}}, \hat{\boldsymbol{\mu}}^{\mathrm{pu}}_{\mathrm{RC+PM}}\right]\right] + \mathrm{h.c.}\right),
\end{aligned} \tag{A29}$$

where we have introduced the nonhermitian resonant dipole operator

$$\hat{\boldsymbol{\mu}}^{\mathrm{pu}}_{\mathrm{RC+PM}} := \sum_{k>l} \tilde{E}^{\mathrm{pu}}(\omega_{kl}) \hat{\mu}^{\mathrm{pu}}_{kl} |k\rangle\langle l|,$$

which can also be obtained by applying the RC to the nonhermitian dipole operator within the RWA, $\hat{\boldsymbol{\mu}}^{\mathrm{pu}}_{\mathrm{RWA}} := \sum_{k>l} \hat{\mu}^{\mathrm{pu}}_{kl} |k\rangle\langle l|$. In the derivation of Eq. (A29), we have also assumed that frequencies of all transitions due to non-Condon effects are much smaller than the carrier frequency of the pulse; this assumption is very well satisfied in molecules. Finally, note that if the initial state $\hat{\boldsymbol{\rho}}$ is in the electronic ground state ($\hat{\boldsymbol{\rho}} = \hat{\rho}_{00} |0\rangle\langle 0|$), then $\hat{\boldsymbol{\rho}}^{\mathrm{pu}}_{\mathrm{NOP+USP+RC}} = \hat{\boldsymbol{\rho}}^{\mathrm{pu}}_{\mathrm{NOP+USP+RC+PM}}$, and that is why we could use $\hat{\boldsymbol{\rho}}^{\mathrm{pu}}_{\mathrm{NOP+USP+RC}}$ in the main text.

Now let us turn to the treatment of the probe pulse and of the final spectrum. Using the Fourier cross-correlation theorem, the spectrum (A20) can be re-expressed as

$$\sigma(\omega, \tau) = \frac{4\pi\omega}{c} |\tilde{E}^{\mathrm{pr}}(\omega)|^{-2} \frac{1}{2\pi} \mathrm{Im}\, \tilde{C}_{E^{\mathrm{pr}} \delta P}(\omega), \tag{A30}$$

where the cross-correlation between E^{pr} and δP is defined as

$$C_{E^{\mathrm{pr}} \delta P}(t) := \int_{-\infty}^{\infty} dt_4 E^{\mathrm{pr}}(t_4 - t)^* \delta P(t_4) \tag{A31}$$

and the argument τ was suppressed for simplicity. Using the TDPT and NOP approximation, we can replace $\delta P(t_4)$ with $\delta P^{(3)}_{\mathrm{NOP}}(t_4)$ from Eqs. (A25) and (A26),

$$\begin{aligned}
&\delta P^{(3)}_{\mathrm{NOP}}(t_4) \\
&\quad = \frac{i}{\hbar} \int_{-\infty}^{t_4} dt_3 E^{\mathrm{pr}}(t_3) \,\mathrm{Tr}\left\{\hat{\boldsymbol{\mu}}^{\mathrm{pr}}(t_4) \left[\hat{\boldsymbol{\mu}}^{\mathrm{pr}}(t_3), \hat{\boldsymbol{\rho}}^{\mathrm{pu}}_{\mathrm{NOP}}\right]\right\} \\
&\quad = \frac{i}{\hbar} \int_{0}^{\infty} dt' E^{\mathrm{pr}}(t_4 - t') \,\mathrm{Tr}\left\{\hat{\boldsymbol{\mu}}^{\mathrm{pr}}(t_4) \left[\hat{\boldsymbol{\mu}}^{\mathrm{pr}}(t_4 - t'), \hat{\boldsymbol{\rho}}^{\mathrm{pu}}_{\mathrm{NOP}}\right]\right\},
\end{aligned} \tag{A32}$$

where we changed integration variables from t_3 to $t' := t_4 - t_3$. Now we also make the USP approximation for the probe

This article is copyrighted as indicated in the article. Reuse of AIP content is subject to the terms at: http://scitation.aip.org/termsconditions. Downloaded to IP: 128.178.54.130 On: Fri, 03 Oct 2014 12:49:48

pulse, consisting in replacing the evolving dipole moment operators $\hat{\boldsymbol{\mu}}^{\rm pr}(t_4)$ and $\hat{\boldsymbol{\mu}}^{\rm pr}(t_4 - t')$ with

$$\hat{\boldsymbol{\mu}}^{\rm pr}_{\rm USP}(t_4) := \sum_{kl} \mu^{\rm pr}_{kl}(\tau + t')|k\rangle\langle l| e^{i\omega_{kl}(t_4 - t' - \tau)}$$

and

$$\hat{\boldsymbol{\mu}}^{\rm pr}_{\rm USP}(t_4 - t') := \sum_{mn} \mu^{\rm pr}_{mn}(\tau)\,|m\rangle\langle n| e^{i\omega_{mn}(t_4 - t' - \tau)}, \quad \text{(A33)}$$

where we used that the peak of the probe pulse arrives at time $t_4 = \tau + t'$ since the probe pulse $E^{\rm pr}(t_4 - t')$ in Eq. (A32) is shifted by t'. Substituting $\delta P^{(3)}_{\rm NOP}(t_4)$ from Eq. (A32), and $\hat{\boldsymbol{\mu}}^{\rm pr}_{\rm USP}(t_4)$ and $\hat{\boldsymbol{\mu}}^{\rm pr}_{\rm USP}(t_4 - t')$ from Eq. (A33) into Eq. (A31) for $C_{E^{\rm pr}\delta P}(t)$, Fourier expanding the real fields $E^{\rm pr}(t_4 - t)^* = E^{\rm pr}(t_4 - t)$ and $E^{\rm pr}(t_4 - t')$, and Fourier transforming the resulting $C^{(3)}_{E^{\rm pr}\delta P,{\rm NOP+USP}}(t)$, we arrive at

$$\begin{aligned}\tilde{C}^{(3)}_{E^{\rm pr}\delta P,{\rm NOP+USP}}(\omega) &= \frac{1}{2\pi}\int_{-\infty}^{\infty}dt\int_{-\infty}^{\infty}dt_4\int_{-\infty}^{\infty}d\omega_4\tilde{E}^{\rm pr}(\omega_4)\int_0^{\infty}dt'\int_{-\infty}^{\infty}d\omega_3\tilde{E}^{\rm pr}(\omega_3)\\ &\quad\times\sum_{klmn} D_{klmn}\left(t'\right)e^{i\phi_{\rm I}}, \end{aligned}\quad \text{(A34)}$$

where

$$\begin{aligned} D_{klmn}(t') &:= \frac{i}{\hbar}\,{\rm Tr}\left[\hat{\mu}^{\rm pr}_{kl}(\tau+t')|k\rangle\langle l|, \left[\hat{\mu}^{\rm pr}_{mn}(\tau)|m\rangle\langle n|, \hat{\boldsymbol{\rho}}^{\rm pu}_{\rm NOP}\right]\right],\\ \phi_{\rm I} &:= \omega t - \omega_4(t_4 - t) - \omega_3(t_4 - t')\\ &\quad + (\omega_{kl} + \omega_{mn})(t_4 - t' - \tau)\\ &= (\omega + \omega_4)t + (\omega_{kl} + \omega_{mn} - \omega_3 - \omega_4)t_4\\ &\quad + (\omega_3 - \omega_{kl} - \omega_{mn})t' - (\omega_{kl} + \omega_{mn})\tau. \end{aligned}\quad \text{(A35)}$$

Integration over t and t_4 gives

$$\begin{aligned}\tilde{C}^{(3)}_{E^{\rm pr}\delta P,{\rm NOP+USP}}(\omega) &= 2\pi\int_0^{\infty}dt'\int_{-\infty}^{\infty}d\omega_4\tilde{E}^{\rm pr}(\omega_4)\int_{-\infty}^{\infty}d\omega_3\tilde{E}^{\rm pr}(\omega_3)\\ &\quad\times\sum_{klmn} D_{klmn}(t')\delta(\omega+\omega_4)\delta(\omega_{kl}+\omega_{mn}-\omega_3-\omega_4)e^{i\phi_{\rm II}},\\ \phi_{\rm II} &:= (\omega_3 - \omega_{kl} - \omega_{mn})t' - (\omega_{kl} + \omega_{mn})\tau, \end{aligned}$$

allowing a trivial integration over ω_4 and ω_3, which yields

$$\begin{aligned}\tilde{C}^{(3)}_{E^{\rm pr}\delta P,{\rm NOP+USP}}(\omega) &= 2\pi\int_0^{\infty}dt'\sum_{klmn} D_{klmn}\left(t'\right)\tilde{E}^{\rm pr}(-\omega)\\ &\quad\times\tilde{E}^{\rm pr}(\omega + \omega_{kl} + \omega_{mn})e^{i\omega t' - (\omega_{kl} + \omega_{mn})\tau}. \end{aligned}$$

Since the probe pulse is centered at τ, it is more convenient to work with $E^{\rm pr}_0(t) := E^{\rm pr}(t + \tau)$, which is centered at $t = 0$ and whose Fourier transform satisfies $\tilde{E}^{\rm pr}(\omega) = \tilde{E}^{\rm pr}_0(\omega)e^{i\omega\tau}$. As a result, we find

$$\begin{aligned}\tilde{C}^{(3)}_{E^{\rm pr}\delta P,{\rm NOP+USP}}(\omega) &= 2\pi\int_0^{\infty}dt'\sum_{klmn} D_{klmn}(t')\tilde{E}^{\rm pr}_0(-\omega)\tilde{E}^{\rm pr}_0(\omega+\omega_{kl}+\omega_{mn})e^{i\omega t'}. \end{aligned}\quad \text{(A36)}$$

Now let us assume that the laser field is almost in resonance with one of the electronic transitions of interest, i.e., $\omega \approx -\omega_{kl}$ (or, equivalently, $\omega \approx \omega_{mn}$). Under this RC,

$$\begin{aligned}\tilde{C}^{(3)}_{E^{\rm pr}\delta P,{\rm NOP+USP+RC}}(\omega) &= 2\pi\int_0^{\infty}dt'\sum_{klmn} D_{klmn}\left(t'\right)\tilde{E}^{\rm pr}_0(\omega_{kl})\tilde{E}^{\rm pr}_0(\omega_{mn})e^{i\omega t'}\\ &= \frac{2\pi i}{\hbar}\int_0^{\infty}dt'\,{\rm Tr}\left\{\hat{\boldsymbol{\mu}}^{\rm pr}_{\rm RC}(\tau + t')\left[\hat{\boldsymbol{\mu}}^{\rm pr}_{\rm RC}(\tau), \hat{\boldsymbol{\rho}}^{\rm pu}_{\rm NOP}\right]\right\}\\ &= \frac{2\pi i}{\hbar}\int_0^{\infty}dt'\,{\rm Tr}\left\{\hat{\boldsymbol{\mu}}^{\rm pr}_{\rm RC}(t')\left[\hat{\boldsymbol{\mu}}^{\rm pr}_{\rm RC}, \hat{\boldsymbol{\rho}}^{\rm pu}_{\rm NOP}(\tau)\right]\right\}, \end{aligned}\quad \text{(A37)}$$

where we used the cyclic property of the trace (on the last line) and introduced the resonant dipole moment

$$\hat{\boldsymbol{\mu}}^{\rm pr}_{\rm RC} := \sum_{kl}\tilde{E}^{\rm pr}(\omega_{kl})\hat{\mu}^{\rm pr}_{kl}|k\rangle\langle l|. \quad \text{(A38)}$$

Substitution of $\tilde{C}^{(3)}_{E^{\rm pr}\delta P,{\rm NOP+USP+RC}}(\omega)$ from Eq. (A37) into Eq. (A30) gives the desired expression for the differential pump-probe spectrum

$$\begin{aligned}\sigma^{(3)}(\omega,\tau) &= \frac{4\pi\omega}{\hbar c}|\tilde{E}^{\rm pr}_0(\omega)|^{-2}\\ &\quad\times{\rm Re}\int_0^{\infty}\left[C^{(3)}_{\mu^{\rm pr}_{\rm RC},\tau}\left(t'\right)^* - C^{(3)}_{\mu^{\rm pr}_{\rm RC},\tau}\left(t'\right)\right]e^{i\omega t'}dt', \end{aligned}\quad \text{(A39)}$$

where the resonant dipole autocorrelation function is

$$C^{(3)}_{\mu^{\rm pr}_{\rm RC},\tau}\left(t'\right) := {\rm Tr}\left[\hat{\boldsymbol{\rho}}^{\rm pu}_{\rm NOP}(\tau)\,\hat{\boldsymbol{\mu}}^{\rm pr}_{\rm RC}\hat{\boldsymbol{\mu}}^{\rm pr}_{\rm RC}\left(t'\right)\right]. \quad \text{(A40)}$$

For ultrashort pump pulses resonant with some electronic transitions, one may also replace $\hat{\boldsymbol{\rho}}^{\rm pu}_{\rm NOP}$ with $\hat{\boldsymbol{\rho}}^{\rm pu}_{\rm NOP+USP+RC+PM}$ from Eq. (A29).

The result (A39) generalizes the "standard" expression (17) since it still depends on the probe field. As mentioned for pump pulses in Sec. V, for sinc pulses the Fourier transform $\tilde{E}^{\rm pr}_0(\omega)$ is a simple box function, the cancellation of the probe field occurs exactly and one obtains the spectrum (17) with the correlation function (18). More generally, the cancellation occurs approximately also for other ultrashort pulse shapes since for resonant transitions, one must have approximately $\omega_{kl} + \omega_{mn} \approx 0$ so $\tilde{E}^{\rm pr}_0(-\omega)\tilde{E}^{\rm pr}_0(\omega + \omega_{kl} + \omega_{mn}) \approx \tilde{E}^{\rm pr}_0(-\omega)\tilde{E}^{\rm pr}_0(\omega)$ in Eq. (A36), resulting again in the spectrum of Eq. (17).

Finally, let us note that in practice, one can replace $\hat{\boldsymbol{\mu}}^{\rm pr}$ with $\hat{\boldsymbol{\mu}}^{\rm pr}_{\rm cutoff} = \hat{\boldsymbol{\mu}}^{\rm pr}$, where $\hat{\mu}^{\rm pr}_{\rm cutoff,kl} = \hat{\mu}^{\rm pr}_{kl}$ for states with transition frequency within the spectral range of the pulse ($\omega_{kl} \in B^{\rm pr}$) and $\hat{\mu}^{\rm pr}_{\rm cutoff,kl} = 0$ otherwise. Although the cross-section for a transition with frequency ω_{kl} outside of the spectral range of the probe may be large (and, due to cancellation of $|\tilde{E}^{\rm pr}_0(\omega)|^2$, in our limit approximately independent of the

This article is copyrighted as indicated in the article. Reuse of AIP content is subject to the terms at: http://scitation.aip.org/termsconditions. Downloaded to IP: 128.178.54.130 On: Fri, 03 Oct 2014 12:49:48

probe field), it cannot be measured with a probe field of a given spectral range if $2\pi\,|\tilde{E}^{\rm pr}(\omega_{kl})|^2$ is lower than the lowest measurable intensity in the experiment. Obviously, using $\hat{\boldsymbol{\mu}}^{\rm pr}_{\rm cutoff}$ enormously simplifies calculations.

[1] P. Atkins and J. De Paula, *Physical Chemistry*, 8th ed. (Oxford University Press, 2006).
[2] T. Zimmermann and J. Vaníček, J. Chem. Phys. **136**, 094106 (2012).
[3] T. Zimmermann and J. Vaníček, J. Chem. Phys. **137**, 22A516 (2012).
[4] T. Zimmermann and J. Vaníček, J. Chem. Phys. **132**, 241101 (2010).
[5] W. Domcke, H. Köppel, and L. Cederbaum, Mol. Phys. **43**, 851 (1981).
[6] W. Domcke and G. Stock, Adv. Chem. Phys. **100**, 1 (1997).
[7] J. Vaníček and E. J. Heller, Phys. Rev. E **68**, 056208 (2003).
[8] J. Vaníček, Phys. Rev. E **70**, 055201 (2004).
[9] J. Vaníček, Phys. Rev. E **73**, 046204 (2006).
[10] A. Peres, Phys. Rev. A **30**, 1610 (1984).
[11] S. Mukamel, J. Chem. Phys. **77**, 173 (1982).
[12] N. E. Shemetulskis and R. F. Loring, J. Chem. Phys. **97**, 1217 (1992).
[13] J. M. Rost, J. Phys. B **28**, L601 (1995).
[14] Z. Li, J.-Y. Fang, and C. C. Martens, J. Chem. Phys. **104**, 6919 (1996).
[15] S. A. Egorov, E. Rabani, and B. J. Berne, J. Chem. Phys. **108**, 1407 (1998).
[16] Q. Shi and E. Geva, J. Chem. Phys. **122**, 064506 (2005).
[17] Q. Shi and E. Geva, J. Chem. Phys. **129**, 124505 (2008).
[18] M. Wehrle, M. Šulc, and J. Vaníček, Chimia **65**, 334 (2011).
[19] M. Šulc and J. Vaníček, Mol. Phys. **110**, 945 (2012).
[20] Q. Shi and E. Geva, J. Phys. Chem. A **108**, 6109 (2004).
[21] W. H. Miller and F. T. Smith, Phys. Rev. A **17**, 939 (1978).
[22] L. M. Hubbard and W. H. Miller, J. Chem. Phys. **78**, 1801 (1983).
[23] H. Wang, X. Sun, and W. H. Miller, J. Chem. Phys. **108**, 9726 (1998).
[24] E. Zambrano and A. M. Ozorio de Almeida, Phys. Rev. E **84**, 045201 (2011).
[25] E. Zambrano, M. Šulc, and J. Vaníček, J. Chem. Phys. **139**, 054109 (2013).
[26] M. Šulc, H. Hernandez, T. J. Martínez, and J. Vaníček, J. Chem. Phys. **139**, 034112 (2013).
[27] L. Kocia and E. J. Heller, J. Chem. Phys. **139**, 124110 (2013).
[28] A. S. Petit and J. E. Subotnik, J. Chem. Phys. **141**, 014107 (2014).
[29] C. Mollica and J. Vaníček, Phys. Rev. Lett. **107**, 214101 (2011).
[30] X. Sun and W. H. Miller, J. Chem. Phys. **106**, 6346 (1997).
[31] M. Thoss, W. H. Miller, and G. Stock, J. Chem. Phys. **112**, 10282 (2000).
[32] J. C. Burant and V. S. Batista, J. Chem. Phys. **116**, 2748 (2002).
[33] A. Kondorskiy and H. Nakamura, J. Chem. Phys. **120**, 8937 (2004).
[34] Y. Wu and M. F. Herman, J. Chem. Phys. **123**, 144106 (2005).
[35] W. H. Miller, J. Phys. Chem. A **113**, 1405 (2009).
[36] E. J. Heller, B. Segev, and A. V. Sergeev, J. Phys. Chem. B **106**, 8471 (2002).
[37] F. Lahmani and N. Ivanoff, J. Phys. Chem. **76**, 2245 (1972).
[38] E. F. Zalewski, D. S. McClure, and D. L. Narva, J. Chem. Phys. **61**, 2964 (1974).
[39] I. Suzuka, N. Mikami, and M. Ito, J. Mol. Spectrosc. **52**, 21 (1974).
[40] D. L. Narva and D. S. McClure, Chem. Phys. **11**, 151 (1975).
[41] I. Yamazaki, T. Murao, T. Yamanaka, and K. Yoshihara, Faraday Discuss. Chem. Soc. **75**, 395 (1983).
[42] W. M. van Herpen, P. A. M. Uijt de Haag, and W. L. Meerts, J. Chem. Phys. **89**, 3939 (1988).
[43] K. Innes, I. Ross, and W. R. Moomaw, J. Mol. Spectrosc. **132**, 492 (1988).
[44] L. Wang, H. Kohguchi, and T. Suzuki, Faraday Discuss. **113**, 37 (1999).
[45] V. Stert, P. Farmanara, and W. Radloff, J. Chem. Phys. **112**, 4460 (2000).
[46] Y.-I. Suzuki, T. Fuji, T. Horio, and T. Suzuki, J. Chem. Phys. **132**, 174302 (2010).
[47] R. Schneider and W. Domcke, Chem. Phys. Lett. **150**, 235 (1988).
[48] L. Seidner, G. Stock, A. L. Sobolewski, and W. Domcke, J. Chem. Phys. **96**, 5298 (1992).
[49] C. Woywod, W. Domcke, A. L. Sobolewski, and H.-J. Werner, J. Chem. Phys. **100**, 1400 (1994).
[50] S. Krempl, M. Winterstetter, H. Plöhn, and W. Domcke, J. Chem. Phys. **100**, 926 (1994).
[51] G. Stock, C. Woywod, W. Domcke, T. Swinney, and B. S. Hudson, J. Chem. Phys. **103**, 6851 (1995).
[52] G. A. Worth, H. Meyer, and L. S. Cederbaum, J. Chem. Phys. **105**, 4412 (1996).
[53] A. Raab, G. A. Worth, H.-D. Meyer, and L. S. Cederbaum, J. Chem. Phys. **110**, 936 (1999).
[54] S. Dilthey, S. Hahn, and G. Stock, J. Chem. Phys. **112**, 4910 (2000).
[55] S. Hahn and G. Stock, Phys. Chem. Chem. Phys. **3**, 2331 (2001).
[56] M. Ben-Nun and T. J. Martínez, Adv. Chem. Phys. **121**, 439 (2002).
[57] C. Coletti and G. D. Billing, Chem. Phys. Lett. **368**, 289 (2003).
[58] D. V. Shalashilin and M. S. Child, J. Chem. Phys. **121**, 3563 (2004).
[59] X. Chen and V. S. Batista, J. Chem. Phys. **125**, 124313 (2006).
[60] R. He, C. Zhu, C.-H. Chin, and S. H. Lin, Chem. Phys. Lett. **476**, 19 (2009).
[61] C. Woywod, A. Papp, G. J. Halász, and A. Vibók, Theor. Chem. Acc. **125**, 521 (2010).
[62] T. Shiozaki, C. Woywod, and H.-J. Werner, Phys. Chem. Chem. Phys. **15**, 262 (2013).
[63] S. Mukamel, *Principles of Nonlinear Optical Spectroscopy* (Oxford University Press, 1995).
[64] W. T. Pollard, S. Lee, and R. A. Mathies, J. Chem. Phys. **92**, 4012 (1990).
[65] The Boltzmann factors of excited electronic states are typically negligible.
[66] L. Seidner, G. Stock, and W. Domcke, J. Chem. Phys. **103**, 3998 (1995).
[67] E. Wigner, Phys. Rev. **40**, 749 (1932).
[68] J. C. Tully, J. Chem. Phys. **93**, 1061 (1990).
[69] J. C. Tully, Faraday Discuss. **110**, 407 (1998).
[70] I. V. Aleksandrov, Z. Naturforsch. A **36**, 902 (1981).
[71] W. Boucher and J. Traschen, Phys. Rev. D **37**, 3522 (1988).
[72] C. C. Martens and J. Y. Fang, J. Chem. Phys. **106**, 4918 (1997).
[73] O. V. Prezhdo and V. V. Kisil, Phys. Rev. A **56**, 162 (1997).
[74] R. Kapral and G. Ciccotti, J. Chem. Phys. **110**, 8919 (1999).
[75] J. Caro and L. L. Salcedo, Phys. Rev. A **60**, 842 (1999).
[76] Q. Shi and E. Geva, J. Chem. Phys. **121**, 3393 (2004).
[77] S. A. Egorov, E. Rabani, and B. J. Berne, J. Chem. Phys. **110**, 5238 (1999).
[78] E. Roman and C. C. Martens, J. Chem. Phys. **121**, 11572 (2004).
[79] G. Hanna and E. Geva, J. Phys. Chem. B **113**, 9278 (2009).
[80] D. J. Tannor, *Introduction to Quantum Mechanics: A Time Dependent Perspective* (University Science Books, 2006).
[81] M. D. Feit and J. A. Fleck, Jr., J. Chem. Phys. **78**, 301 (1983).
[82] L. Verlet, Phys. Rev. **159**, 98 (1967).
[83] R. B. Sidje, ACM Trans. Math. Softw. **24**, 130 (1998).
[84] H.-J. Werner, P. J. Knowles, G. Knizia, F. R. Manby, M. Schütz *et al.*, Molpro, version 2010.1, a package of *ab initio* programs, 2010, see http://www.molpro.net.
[85] Note that due to the presence of nonadiabatic couplings even electronic levels which lie outside of the specific energy range may influence the spectrum and care has to be taken as to which states may be neglected.
[86] T. J. Martínez, M. Ben-Nun, and R. D. Levine, J. Phys. Chem. **100**, 7884 (1996).
[87] I. Burghardt, H.-D. Meyer, and L. S. Cederbaum, J. Chem. Phys. **111**, 2927 (1999).
[88] I. Burghardt, K. Giri, and G. A. Worth, J. Chem. Phys. **129**, 174104 (2008).
[89] P. Siegbahn, A. Heiberg, B. Roos, and B. Levy, Phys. Scr. **21**, 323 (1980).
[90] B. O. Roos, P. R. Taylor, and P. E. Siegbahn, Chem. Phys. **48**, 157 (1980).
[91] P. E. M. Siegbahn, J. Almlöf, A. Heiberg, and B. O. Roos, J. Chem. Phys. **74**, 2384 (1981).
[92] U. Werner, R. Mitrić, and V. Bonačić-Koutecký, J. Chem. Phys. **132**, 174301 (2010).
[93] J.-Y. Fang and S. Hammes-Schiffer, J. Phys. Chem. A **103**, 9399 (1999).
[94] G. Granucci, M. Persico, and A. Zoccante, J. Chem. Phys. **133**, 134111 (2010).
[95] R. Kosloff, A. D. Hammerich, and D. Tannor, Phys. Rev. Lett. **69**, 2172 (1992).
[96] In an experiment j with narrow laser beams, $\vec{P}^{\,j}_{\vec{k}^{\rm pr}}$ is the only component of $\vec{P}^{\,j}$ contributing to the spectrum measured in direction $\vec{k}^{\rm pr}$.

This article is copyrighted as indicated in the article. Reuse of AIP content is subject to the terms at: http://scitation.aip.org/termsconditions. Downloaded to IP: 128.178.54.130 On: Fri, 03 Oct 2014 12:49:48